KIMBERLITE SILLS AND DYKES ASSOCIATED WITH THE WESSELTON KIMBERLITE PIPE, KIMBERLEY, SOUTH AFRICA

J.L. WHITE, R.S.J. SPARKS, K. BAILEY
Department of Earth Sciences, University of Bristol, Wills Memorial Building, Bristol, BS8 1RJ, United Kingdom
e-mail: jennywhite1983@hotmail.com; Steve.Sparks@bristol.ac.uk; Ken.Bailey@bristol.ac.uk

W.P. BARNETT
SRK Consulting (Canada) Inc. 2200-1066 West Hastings Street, Vancouver, BC V6E 3X2, Canada
e-mail: wbarnett@srk.com

M. FIELD
Department of Earth Sciences, University of Bristol, Wills Memorial Building, Bristol, BS8 1RJ, United Kingdom
DiaKim Consulting Limited, Mayfield, Wells Road, Wookey Hole, Wells, BA5 1DN, United Kingdom
e-mail: matthew-field@btconnect.com

L. WINDSOR
Department of Earth Sciences, University of Bristol, Wills Memorial Building, Bristol, BS8 1RJ, United Kingdom
e-mail: seroster99@hotmail.com

ABSTRACT
Field relations, petrography and bulk rock geochemistry constrain the emplacement mechanisms and petrogenesis of a kimberlite sill complex exposed in water tunnels at Wesselton Mine, Kimberley. The sill complex, together with associated dykes, is precursor to the main Wesselton pipe and contains:
1. aphanitic kimberlite with a carbonatitic groundmass of calcite, perovskite, spinel, serpentine and phlogopite, with variations from rocks rich in olivine microphenocrysts to rocks with little or no olivine;
2. macrocrystic kimberlite containing entrained harzburgite microxenoliths, olivine macrocrysts and strongly reacted orthopyroxene; and,
3. a 'green' aphanitic kimberlite.

The sills were emplaced as multiple intrusions into the upper Dwyka shales immediately below a Karoo dolerite sill in a zone several metres thick. Emplacement of the sill complex was governed by the rigidity of the dolerite sill, which prevented the magma from breaching the surface. Feeder dykes to the sills were influenced by a regional crustal stress system with the principal vector of horizontal compression being between eastwest and northwest-southeast. Serpentinisation has pseudomorphed olivine, replaced calcite, apatite and phlogopite in the groundmass and thereby changed the bulk compositions. Geochemcal and mineral chemistry data on spinels and phlogopites indicate intrusion of several magma batches with different petrogenetic histories. The magmas are transitional to carbonatite with compositional variations linked to partial melting, assimilation of xenocrysts, entrainment of xenoliths, xenocrysts and macrocryst, fractional crystallization and flow differentiation during ascent and emplacement.
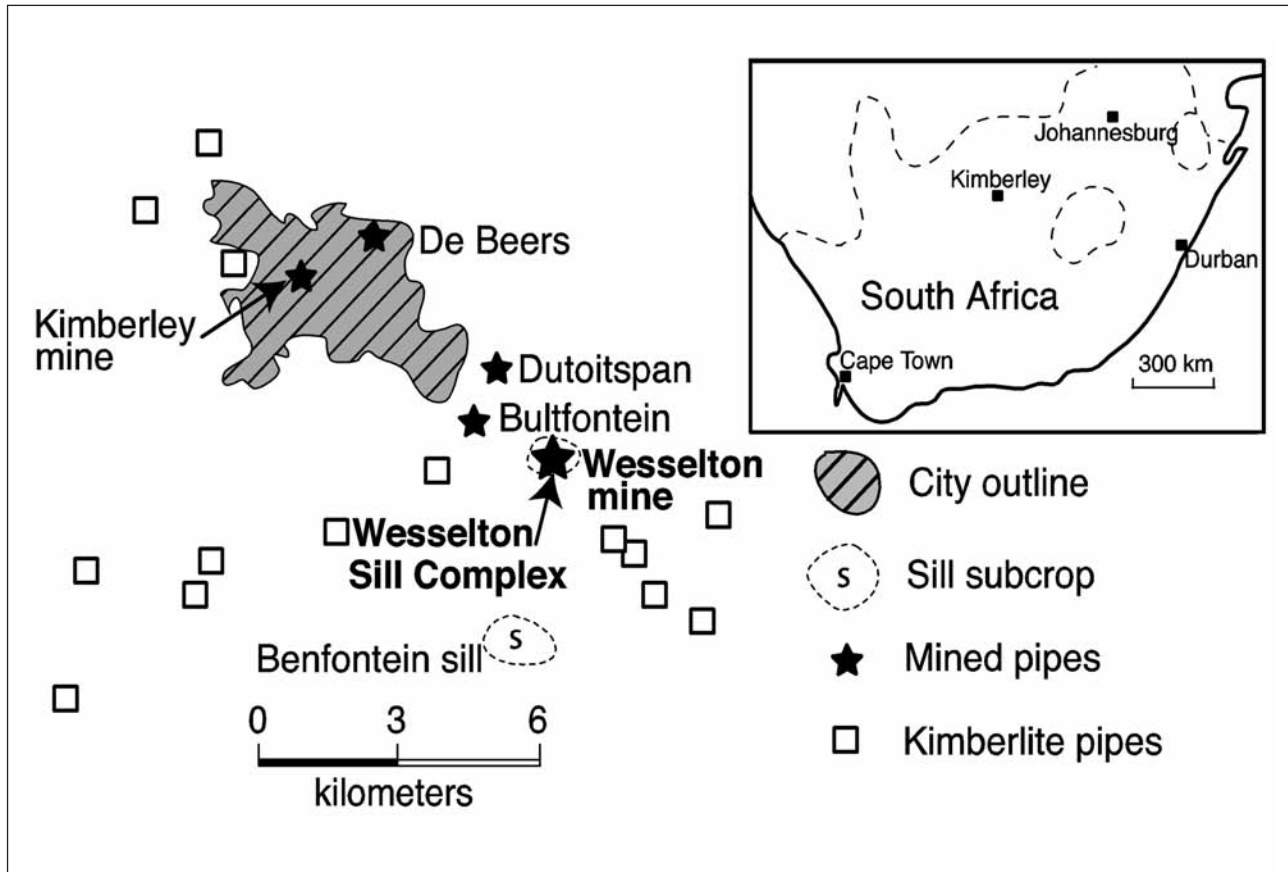
Introduction
The Wessurton sill complex is composed of precursor kimberlite sills and dykes associated with the Wesselton kimberlite pipe, Kimberley, South Africa. This study investigates their intrusion mechanisms, and describes their petrology and geochemistry. Observations are presented that have implications on the emplacement mechanisms of kimberlites. Hypabyssal kimberlites are not brecciated or fluidised during emplacement, so offer potential for constraining the nature of kimberlite magmas, including their physical properties, pristine mineral assemblages and magma compositions. The paper highlights the importance of serpentinisation in altering the bulk composition of kimberlites.

Implications for petrogenetic processes, including evidence for intrusion of several geochemically distinctive magma batches, the relationships between kimberlite and carbonatite magmas, and modification of magma compositions during ascent and emplacement, are discussed.

Geological setting
Wesselton Mine is situated 6.5 km southeast of Kimberley in the Northern Cape Province of South Africa and is one of five major diamondiferous kimberlite pipes (Kimberley, Wesselton, Dutoitspan, De Beers and Bultfontein) within and near the city (Figure 1). The Wesselton pipe is 600 m in diameter at surface level,

Figure 1. *Location of Wesselton Mine, other major kimberlite occurrences around Kimberley, the Wesselton sill complex, and the Benfontein sill. Note the northwest to southeast alignment of the five major diamondiferous kimberlite pipes.*

intruding Archean basement gneisses, andesite lavas and quartzites of the Ventersdorp Supergroup lavas and Karoo Supergroup sedimentary rocks and dolerite intrusive rocks (Figure 2). The pipe is made up of at least ten separate units (Clement, 1982; Shee, 1985), dated at approximately 90.3 ma from a zircon and 88.6 ma from whole rock by the U-Pb method (Davis, 1977; Smith, 1983).

A kimberlite sill complex and associated dykes was discovered by Wagner (1914), mapped by Hill (1977), and described by Clement (1982), Shee (1984; 1985), Mitchell (1984), and Shee et al. (1991). This hypabyssal complex has not been dated radiometrically, but it is cut by the Wesselton pipe (Hill, 1977; Clement, 1982). Gaspar and Wyllie (1984) presented ilmenite and spinel compositions from one of the Wesselton dykes, and there is a considerable amount of mineral chemistry on Wesselton rocks, including the macrocrystic sills and dykes, in Shee (1985).

The kimberlite sills intrude the contact zone between the well-bedded upper Dwyka carbonaceous shales (Lower Karoo Supergroup: ~310 to 280 Ma) and a Karoo dolerite sill (associated with the Upper Karoo Supergroup: ~195 to 135 Ma) (Hill, 1977; Shee, 1985; Mitchell, 1986), and extend over a minimum area of 0.7 km^2 (Clement, 1982). The sills are exposed in metre-wide water drainage tunnels at depths of approximately

40 m below surface level (Figures 2 and 3). The tunnels are concentric around Wesselton pipe and intersect the shale-dolerite contact in several places. The Wesselton Floor and Benfontein Sill complex also occur at the base of the Karoo dolerite sill (Figure 1), suggesting that the dolerite initially prevented kimberlite magma breakthrough to the surface and controlled sill emplacement (Hawthorne, 1968).
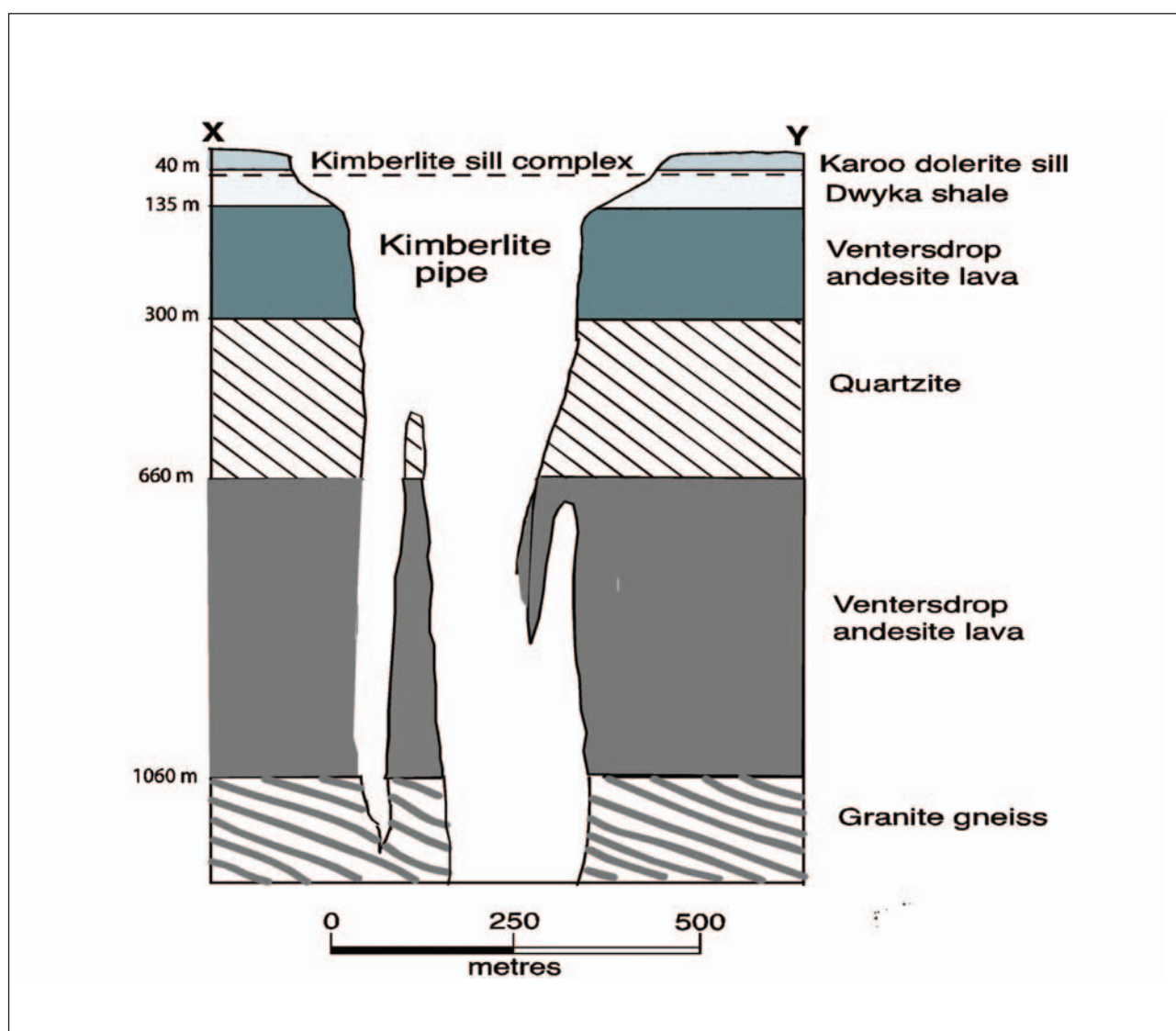
The greater Kimberley area hosts a plethora of kimberlite pipes and dykes intruded during the Cretaceous. Two distinct groups of kimberlite occurrences can be distinguished based on composition and age, namely Group 1 kimberlites that typically intrude between 75 and 100 ma, and Group 2 kimberlites that were more prolific between 114 and 150 ma (Field et al., 2008). The five major Kimberley pipes are all regarded as Group 1 type kimberlites with ages that cluster around 90 Ma.

During the Cretaceous the near-surface geology of southern Africa was dominated by the rock of the Karoo Supergroup. These rocks were deposited in a foreland basin over southern Gondwana during the Late Paleozoic to Early Mesozoic (Tankard et al., 1982; De Wit, 2007; Hanson et al., 2009). By Cretaceous times, prior to and after the separation of Africa from South America at ~132 to 125 Ma, the southern African continent underwent extensive uplift and erosion.
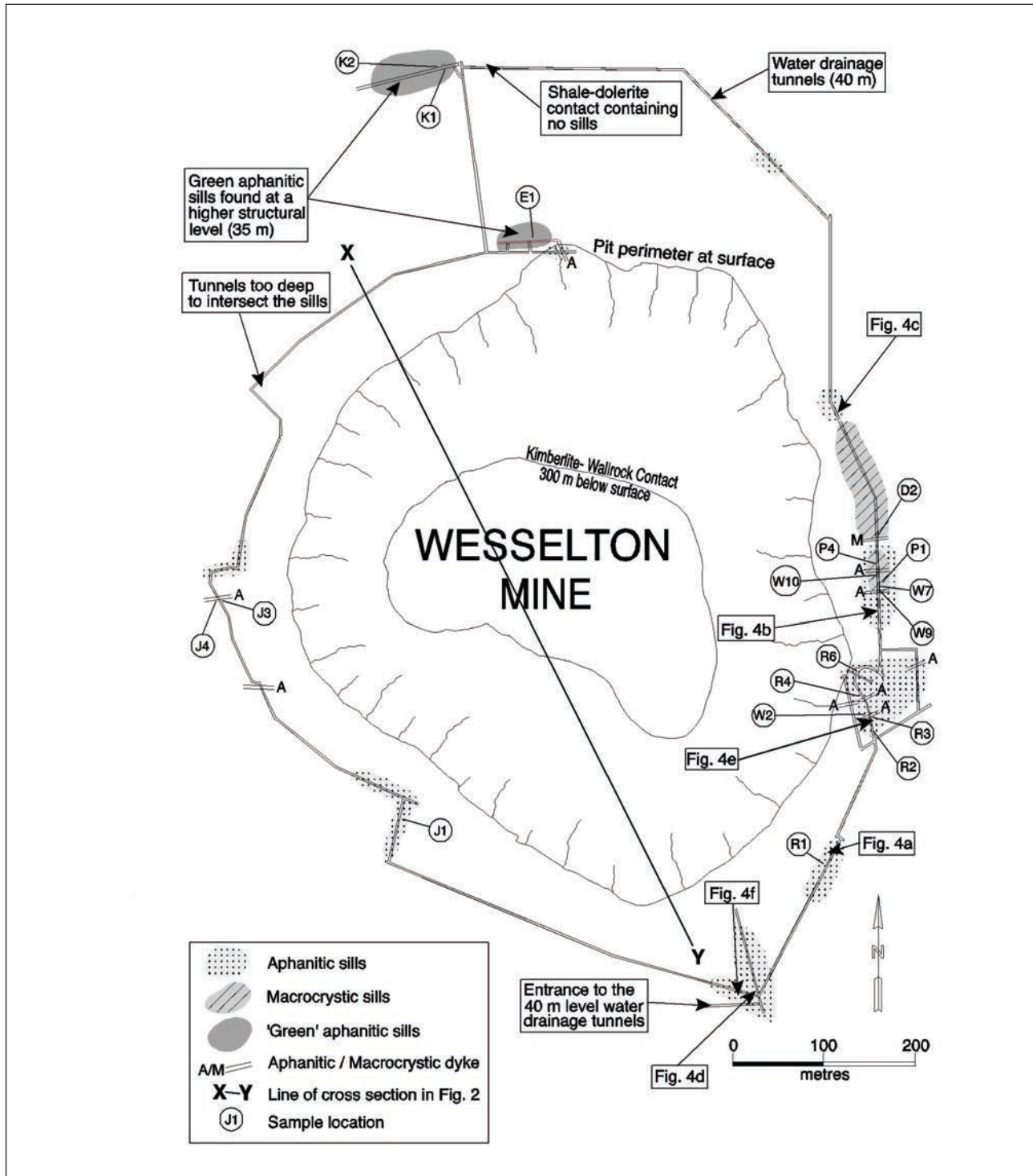
Kimberlite pipes intruded the crust and were eroded contemporaneously with a retreating escarpment of Karoo basalts and steadily eroded stratigraphy. Hanson et al. (2009) correlate the crustal xenoliths incorporated and preserved during the emplacement of various kimberlite pipes to the chemostratigraphy of the Karoo basin, in order to track the erosion rate and estimate depths of pipe erosion.

Based on this reconstruction of the erosional history of southern Africa, Hanson et al. (2009) estimate the Group 1 Kimberley pipes to have undergone ~850 m of erosion; less than the 1400 m estimated by Hawthorne (1975). The Kimberley pipes are therefore regarded to preserve the mid to lower pipe diatreme and root zones (Hawthorne, 1975; Field and Scott-Smith, 1999; Mitchell et al., 2009). The Wesselton sills can be considered to have been about 900 m below the surface at the time of pipe emplacement.

The association of the abundant Cretaceous kimberlites across southern Africa with the regional tectonic uplift and extensional rift tectonic conditions is not considered coincidental (Dawson, 1970; Jelsma et al., 2004; De Wit, 2007; Moore et al., 2008; Jelsma et al., 2009). Extensional or transtensional strain conditions are favourable, possibly even necessary, to aid kimberlite dyke propagation through the thick diamond-bearing lithosphere of the Kaapvaal craton. In addition, periods of kimberlite infiltration through the lithosphere are regarded as time-markers, indicating periods when the lithosphere underwent minor tectonic re-organization (Bailey and Woolley, 1995; Jelsma et al., 2009). Such changes in plate velocity and direction cause differential stress variations across the plates, resulting in local strain concentrated on pre-existing lithospheric structural weaknesses (Jelsma et al., 2004; Barnett, 2006).

Figure 2. *Cross-section X-Y through Wesselton Pipe; the location of the section is shown in Figure 3. The kimberlite sill complex intrudes the upper Dwyka shales immediately below a Karoo dolerite sill and is exposed in the 40 m water drainage tunnels. Note that the kimberlite pipe is well defined down to a depth of 1060 m, below which depth the geology is inferred.*

.**Figure 3.** *Geological map of the 40 m water drainage tunnels, showing the locations of the three groups of kimberlite sills and dykes. Sample locations are also shown.*

The five Kimberley pipes cluster along a broad west-northwest to east-southeast trending zone (Bosch and Visser, 1993) (Figure 1). This trend has been statistically distinguished from the distribution of Group 1 Cretaceous kimberlites (Vearncombe and Vearncombe, 2002; Barnett, 2006), and the trend is observed in the Lesotho kimberlite occurrences (Nixon and Kresten, 1973; Jelsma et al., 2009). The trend also reflects the dominant orientation of the principal component of maximum compressive stress regionally across southern Africa through the Late Cretaceous to the present day (Andreoli et al., 1996). In the greater Kimberley area crustal aerial photograph lineaments (Greeff, 1968) and aeromagnetic lineaments (Barnett, 2006) strike between west-northwest to east-southeast and northwest-southeast, likely representing crustal structures.

The trend of a prominent kimberlite dyke through Kimberley mine is west-northwest to east-southeast. The pipes also intersect two other major fracture and mafic dyke directions: northeast-southwest and east-west (Visser 1984). Dawson (1970) notes that the east-west direction coincides with the foliation in the basement granite-gneiss.

Geology and field relations
Field characteristics of the sills

In outcrop and hand specimen, the sills and dykes vary in characteristics due to variable alteration, different intrusion styles and different petrological varieties. Three main varieties of intrusive rock are identified, the first two of which were recognised by Hill (1977).

The first variety, termed *macrocrystic kimberlite*, contains macrocrysts and xenolithic fragments of shale and harzburgite set in a fine-grained matrix. The non-genetic term "macrocryst" describes crystals which are visible to the unaided eye and are significantly larger than the surrounding matrix (>2 mm in size) (Shee et al., 1991). The macrocrystic sill is hard and dark grey to black in colour with macrocrysts up to 2 cm in size. The larger macrocrysts are composed predominantly of olivine and minor enstatite, and are interpreted as derived by break-up of harzburgite. The maximum macrocryst:matrix ratio is 30:70.

The second variety, termed *aphanitic kimberlite*, is fine-grained and light brown to buff, but mid-grey where fresher. The aphanitic kimberlite does not contain any macrocrysts, but is commonly microporphyritic, due to the presence of numerous small serpentinised microphenocrysts after olivine. The aphanitic kimberlite varies from those with abundant olivine microphenocrysts (less than 1 mm in size and spaced about 1 to 2 mm apart) to rocks with no olivine microphenocrysts.

A third variety, termed *green aphanitic kimberlite*, is distinguished by its green weathered surface. The green aphanitic kimberlite contains millimetre sized olivine microphenocrysts (mostly serpentinised) surrounded by a fine grey matrix. Veins of calcite, 0.5 to 3 mm in width, commonly cut this variety.

Sill location and intrusion form

The sills intrude a vertically narrow zone, up to 8 m thick, which follows the undulations of the base of the dolerite sill. Both the aphanitic and macrocrystic sills are found in the eastern tunnels (Figure 3), but only some aphanitic sills outcrop in the west, because the water tunnels are too deep to intersect the shale-dolerite. The green aphanitic sill is found in the northern tunnels (Figure 3).

The aphanitic sills are typically a few centimetres thick, but can vary from a few millimetres up to a metre. No contact effects were observed in the country rock adjacent to the sills. The sills are commonly concordant with the bedding in the shale (Figure 4a), but locally split or bifurcate around blocks of host rock, and are transgressive across beds in steps and ramps (Figure 4b). The sills commonly show en-echelon or segmented geometry, where one sill tapers out and another sill develops above or below (Figure 4c). Several sills can form with intervening shale screens (Figure 4a). Where the aphanitic sills are found with the macrocrystic sill, the aphanitic sills occur below the macrocrystic sill, so occupy the lower part of the kimberlite intrusive zone, which is dominantly just below the shale-dolerite contact in a 2 to 3 m zone. The sills rarely intrude directly at the shale-dolerite contact suggesting that the shale is harder here (Figure 4d) as a consequence of contact metamorphism by the dolerite prior to kimberlite intrusion. The sills locally intrude into the dolerite along weaknesses and joint planes, up to 1 m above the contact. We observed one example of an aphanitic sill containing no olivine microphenocrysts cutting an aphanitic dyke containing olivine microphenocrysts.

The aphanitic sills are fed and linked by aphanitic dykes. The dyke widths vary between 7 cm and 135 cm, but are predominantly 10 to 40 cm wide, and are commonly perpendicular to the pipe margin (Figure 3). The dykes can have a planar form or very irregular margins. Where the intrusion margins are irregular, they tend to match up on either side of the dykes, implying pure dilation. Several of the dykes show complex horizontal and vertical kimberlite offshoots extending about 1 m either side of the main dyke. It is common for the dykes to bake the adjacent shales.
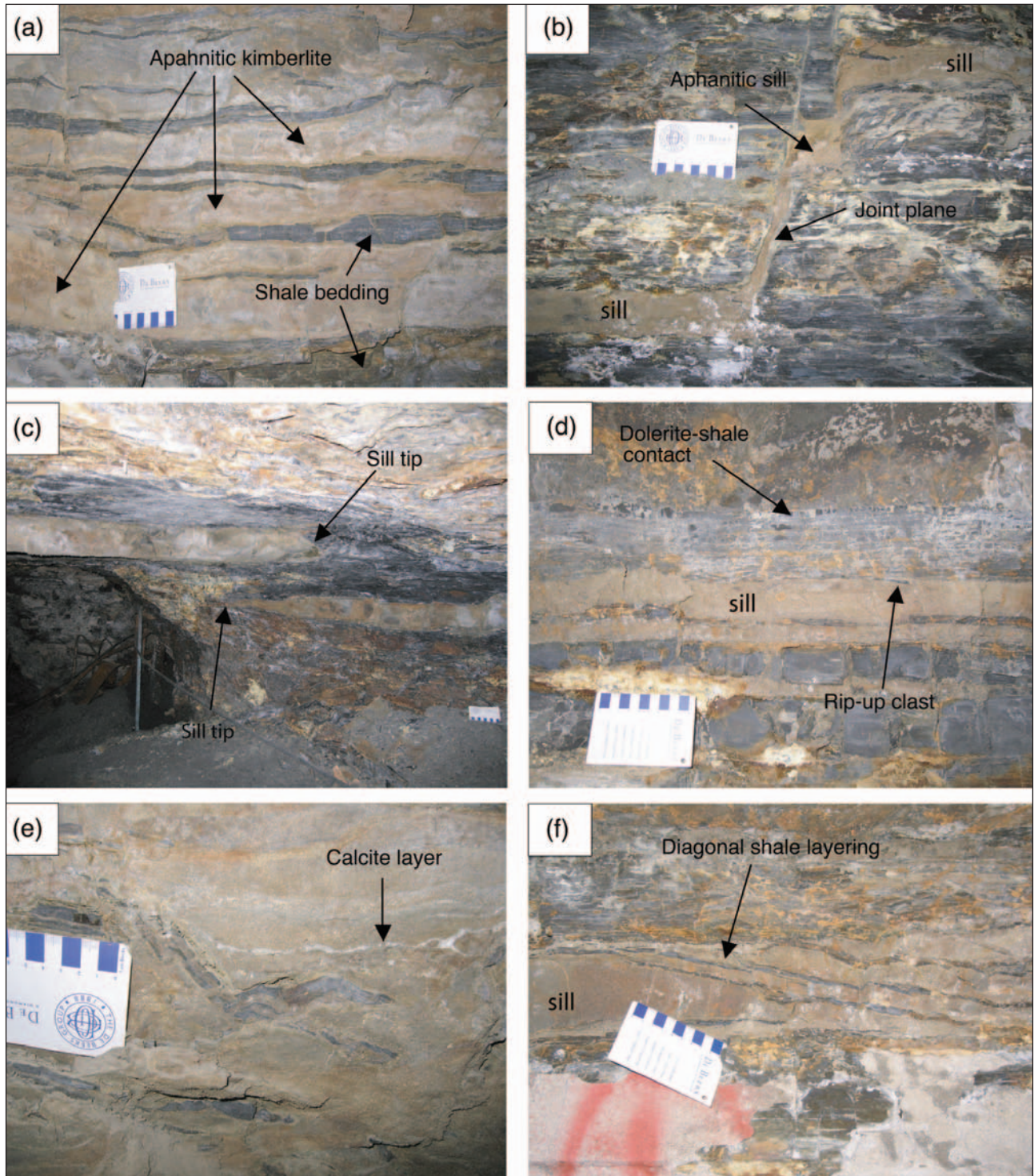
The macrocrystic sill is massive with a minimum thickness of 30 cm and a reported maximum of about 5 m (Hill, 1977). The macrocrystic sill cross cuts the aphanitic sills and dykes. The contact is sharp, indicating that the earlier sills and dykes consolidated before its intrusion. The macrocrystic sill is planar and does not change thickness rapidly or split. In places the macrocrystic sill has a laccolithic shape and has caused the overlying shale to bend upwards. The macrocrystic feeder dykes are up to 32 cm in width, but typically 10 to 20 cm. Macrocrystic dykes and sills contain large, angular shale clasts and are cut by thin calcite veins.

The green aphanitic sill is at least 5 m in thickness, with a maximum thickness of 8 m. The intrusion is massive with planar sides, similar to the macrocrystic variety.

Petrological presented below show that the green aphanitic sill contains xenocrysts of spinel and spinel inclusions in olivine derived from the macrocrystic and aphanitic sills, so it is the youngest intrusion.

Structures in the sills

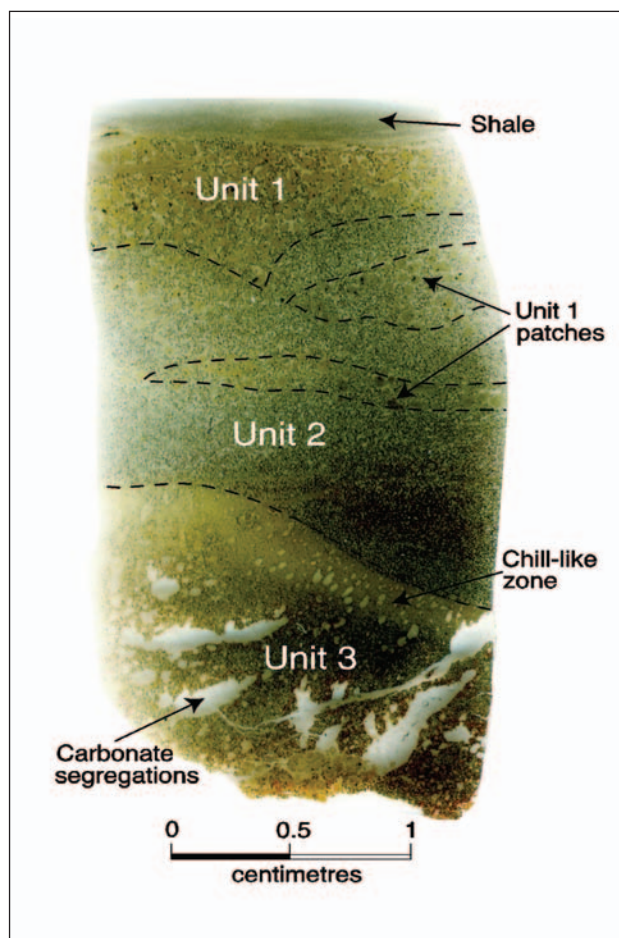Internal layering and contacts. Horizontal layering within the aphanitic sills is recognised by subtle changes in texture and colour (Figure 4e), and by the presence or absence of olivine microphenocrysts. Individual internal units are thin, generally in the order of 1 to 5 cm (Figure 5). The internal contacts (Figure 4e) can be sharp or diffuse (Figures 4e and 5). Cross cutting relationships imply that the aphanitic kimberlite with

Figure 4. (*a*) *Intervening screens of concordant shale and aphanitic kimberlite.* (*b*) *Transgressive aphanitic kimberlite opening up along a near-vertical joint plane.* (*c*) *Segmented aphanitic sill. Note the concordance with the bedding and tapered tips.* (*d*) *Aphanitic sill intruding below the shale-dolerite contact. The shale is harder next to the dolerite, indicative of a baked margin. Note also the small rip up clast on the upper margin of the sill.* (*e*) *Crude horizontal layering in the aphanitic sill. Note the concordant thin calcite-rich layer and the bent shale layer.* (*f*) *Diagonal shale layering in the aphanitic sill. The shale is attached to the country rock at the top and bottom margins of the sill. Scale bar = 10 cm.*

olivine microphenocrysts intruded first, and was later cut by magma batches containing no olivine microphenocrysts. However, intimate layering of olivine-absent, olivine-poor and olivine-rich rocks also indicates contemporaneous injection of the magma variants. Concordant calcite-rich layers are also observed (Figure 4e). Diagonal shale layering is seen, where the shale layer is attached to the country rock at the top and

Figure 5. *Enlarged thin section of the aphanitic sill (sample R6). Units 1-3 are described in the text.*

bottom with the aphanitic sill intruding between septa of shale (Figure 4f).
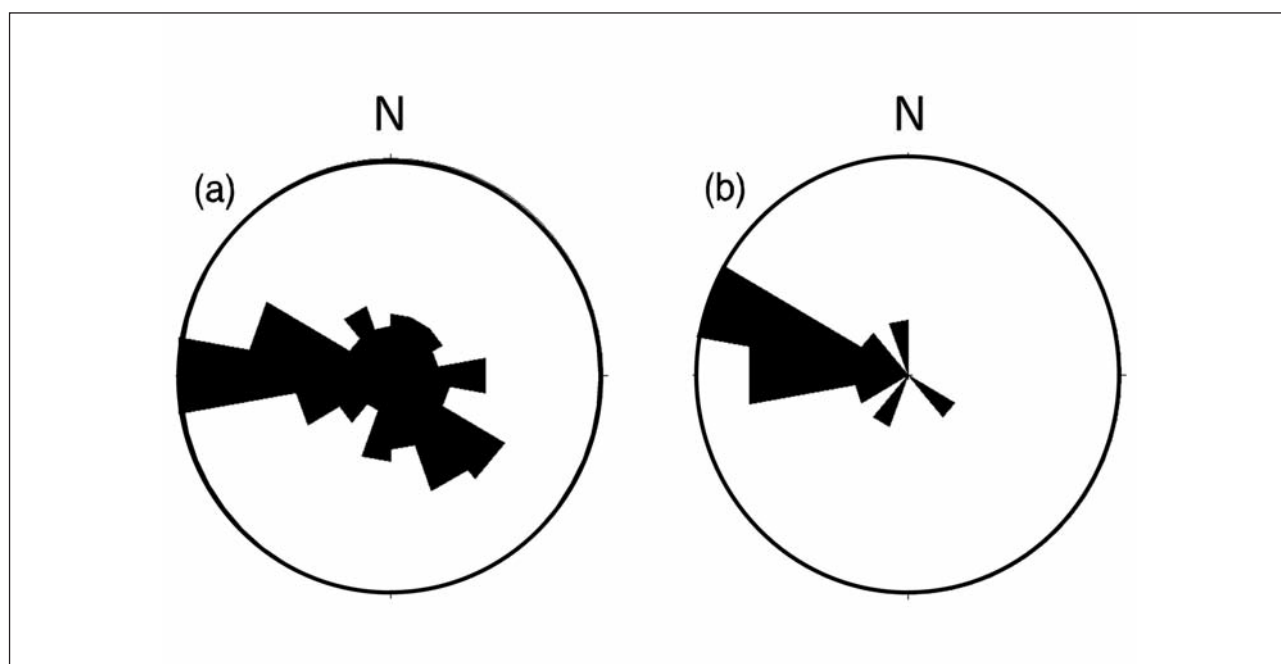
Flow structures
The aphanitic and macrocrystic kimberlite contain shale bedding planes that have been lifted from the margins of the sill by the flow of magma to form typically centimetre sized rip-up clasts (Figure 4d). These features can be used to infer an approximate flow direction for the magma. Imbrication of shale clasts can also infer flow direction. The dominant flow direction is radially from a centre located where the subsequently formed Wesselton pipe is now located. However, close to the dykes inferred directions are not systematic.

Country rock xenoliths
Shale layers usually maintain a horizontal orientation in the aphanitic sills, but some form small scale 'S' and 'Z' bends (Figure 4e) and some have cracks in them, indicative of brittle deformation. Elongate and twisted shale clasts occur in the aphanitic dykes, as well as a 20 cm sized dolerite block. The shale clasts incorporated into the macrocrystic sills and dykes range from small, centimetre sized fragments, to blocks up to 0.5 m. There are also examples of fracture-bounded blocks detached from the hanging wall and incorporated into the sill.

Structural Data
The upper Dwyka shales are flat lying and undisturbed by major faulting or intense folding, although local mild folding is evident. The kimberlite sills are largely conformable with the bedding. There are examples

Figure 6. (**a**) *Rose diagram of the azimuth of the joints measured in the 40 m water tunnels at Wesselton Mine.* (**b**) *Rose diagram of the azimuth of the dykes. Note the dominance of northwest to southeast and east to west trending joints and dykes.*

where the emplacement of the sills has tilted the shale, suggesting that some folding occurred during or after intrusion. The sills predominantly intrude along bedding planes and occasionally intrude along joint planes. The aphanitic sills commonly step up or down along selected joints (Figure 4b), particularly shallow lying ones, but the vertical extent is never more than about half a metre (normally 10 to 20 cm). Some, but not all, of the joints on which the sill steps up or down are filled with a thin layer (<1 cm) of kimberlite, indicating that the joints were present before the magma stagnated and solidified. The dominant azimuth direction of the joints is east to west to northwest to southeast (Figure 6a).

All 15 of the kimberlite dykes are near vertical and 13 of them strike between east to west and northwest to southeast; two dykes intrude approximately north to south. The dykes have a mean azimuth of 278° (Figure 6b). The dykes predominantly lie along joint planes and most of the aphanitic dykes intrude along several joint orientations within a few metres distance. The aphanitic dykes are commonly transgressive with side-steps along the bedding. Joints do not increase in density towards the dykes and therefore no dyke damage zone developed.

A De Beers magnetic survey (internal company report, 2002) reveals a 3 km long positive magnetic anomaly that intersects the eastern and western perimeters of Wesselton pit (Figure 7). This anomaly is interpreted as an eastwest oriented kimberlite dyke. A 1 km diameter zone of magnetic material surrounds the pit and may represent the sills.

Interpretation of field data

The textural variations and cross-cutting relationships indicate that the sill complex was emplaced in several events. The internal textural layering in the aphanitic sills shows that repeated injections occurred almost simultaneously. The very thin intrusions indicate that the aphanitic sills were emplaced as non-violent low viscosity magmas. Hawthorne (1968) suggested that the low viscosity is due to a high volatile content rather than a high intrusion temperature.

The geological relationships of the Wesselton sill complex suggested that the dolerite acted as an effective barrier to kimberlite ascent (Hawthorne, 1968). This interpretation is supported by analogue experiments of Kavanagh et al. (2006) who injected vertical water-filled cracks into two layers of gelatine of contrasted rigidity and density. Sills were only formed in the experiments when the vertical fracture (dyke analogy) intersected a higher rigidity upper layer, where the vertically propagating fracture re-oriented to form a horizontal intrusion (sill analogue) just below the interface between the two layers. Sill intrusion at Wesselton preceded pipe emplacement (Hill, 1977; Clement, 1982). It is possible that the kimberlite magma intruded and sealed the area, resulting in the accumulation of volatiles at the head of the magma column (Clement 1982). Pressure built up, causing the

dolerite to fracture and weaken, and the kimberlite to break through to the surface to initiate pipe formation possibly accompanied by explosive brecciation (Field and Scott-Smith 1999).

The geometry of the sill complex is influenced by the morphology of the host rock, changing stress orientation and the presence of other intrusions or structures (Pollard 1973). The sills dominantly intrude along pre-existing weaknesses, such as the shale bedding and joints. The presence of thin selvages of kimberlite on fractures along which the sill steps up or down indicates that the magma pressure was high enough to dilate the fractures during sill formation. The present state of closure of the joints indicates a subsequent release of pressure. The elongated and twisted shale clasts in the aphanitic dykes were 'sucked' into the dykes from the connecting sills as a result of declining magmatic pressure. Opposing flow directions near the dykes (inferred from rip-up clasts) support this interpretation. We observed one dyke split and intruded along three different joint planes, which were orthogonal to one other. For magma to invade pre-existing weaknesses in different orientations, magma pressure must exceed either the lithostatic pressure or the normal component of the regional stresses resolved on the fracture planes (Delaney et al. 1986). These observations therefore imply high magma pressures. Fluctuating magmatic pressure, the presence of different textural varieties and internal contacts suggest the kimberlite magma was transported in discontinuous batches (Bons et al. 2004).

En-echelon offsets suggest that the local tension direction was oblique to the bedding planes (Rubin 1995). During multiple intrusions it is common for the early intrusions to distort the local stress field, causing local deviations and variations of sill orientations (Menand, 2008). Emplacement of vertical dykes also increases local horizontal stresses normal to the dyke walls, promoting sill development. High horizontal stresses in the host rock of a sill promote fracturing, dilation and buckling of the hanging and footwall of the sill. An example is the diagonal shale layering (Figure 4f). Compression can buckle laminated rocks, so that, if magma subsequently dilates this material, it will preferentially open up along these kinks. The diagonal layering is located in the southern tunnels (Figure 3), lying in an east-west orientation that implies east-west compression. Other similar structures are observed, but in other examples the shale from the top and bottom is not connected. These structures are attributed to a combination of gravitational effects and buckling. Magma flow may cause the shale to bend and break. Entrained shale clasts can easily settle through the low viscosity magma.

The Wesselton sills were affected by a lithostatic load when they were intruded. Doming and fracturing of the shales was evidently limited and a consequence of the radially directed sill intrusion around a centre later replaced by the Wesselton pipe. Structural observations and the magnetic survey show that most of the dykes

Table 1. Modal mineral proportions in area %.

1. spinel-rich aphanitic kimberlite with olivine microphenocrysts (sample R6);

2. spinel-rich aphanitic kimberlite without olivine microphenocrysts (sample R6);

3. Olivine-rich area in aphanitic sill (W2);

4. spinel-poor aphanitic kimberlite with olivine microphenocrysts (sample W1);

5. spinel-poor and olivine-poor aphanitic kimberlite;

6. macrocrystic kimberlite (sample P4);

7. macrocrystic kimberlite (sample W7);

8. macrocrystic kimberlite with maximum harzburgite microxenoliths (sample W8);

9. spinel-rich variety of green aphanitic kimberlite (sample E1).

	1	2	3	4	5	6	7	8	9[d]
Serpentine	42	26	–	–	27	34[c]	47[c]	14[c]	46
Olivine pseudomorph	–	–	14[a]	33[a]	–	–	–	–	–
Rim and distributed serpentine	–	–	20[a]	14[a]	–	–	–	–	–
Calcite	21	26	39	30	33	21	15	12	16
Phlogopite[e]	7	10	11	11	20	7	30	7	7
Spinel	21	26	6	6	9	21	6	12	25
Apatite	4	7	8	5	9	2	4	1	1
Perovskite	5	5	2	1	2	4	2	1	5
Olivine xenocryst	–	–	–	–	–	7	–	36	–
Orthopyroxene	–	–	–	–	–	1	–	17	–

Footnotes: a. Serpentine pseudomorphing olivine was distinguished from disseminated and rim serpentine by image analysis of SEM image. **b**. disseminated serpentine with no olivine pseudomorphs observed. **c**. Disseminated serpentine in the macrocrystic kimberlite is intimately intergrown with a K-rich phyllosilicate, which is included in the mode of serpentine. **d**. Sample E1 contained vein calcite, which made up 7% of the mode but is not included above. **e**. Phlogopite is variably replaced by a smectite mineral, which is included in the modes for phlogopite, noting that pholgopite alteration is minor in the aphanitic samples (1 to 4) but significant in some macrocrystic samples and the green aphanitic variety.

trend east to west to northwest to southeast. Joint distributions also dominantly trend east to west to northwest to southeast. The preferred dilation of structures to produce the dyke trends implies a horizontal regional compressive stress between east to west and northwest to southeast. These joint distributions coincide with the elongation directions of subsurface parts of the Wesselton pipe (Clement 1982), and can be traced across most of South Africa, implying a strong regional control (Greeff 1968; Visser 1984; Andreoli et al., 1996). The observations therefore suggest sill emplacement guided by the contemporaneous stress field but influenced by the orientation of major crustal structures.

The observations of very thin sills with evidence of internal textural layering due to several discrete intrusive events, together with evidence of high magma pressures, place constraints on the dynamic conditions of sill emplacement. A maximum time scale of emplacement is estimated by considering a sill of width, w, and noting that such a sill would be consolidated on a time scale, t, given by
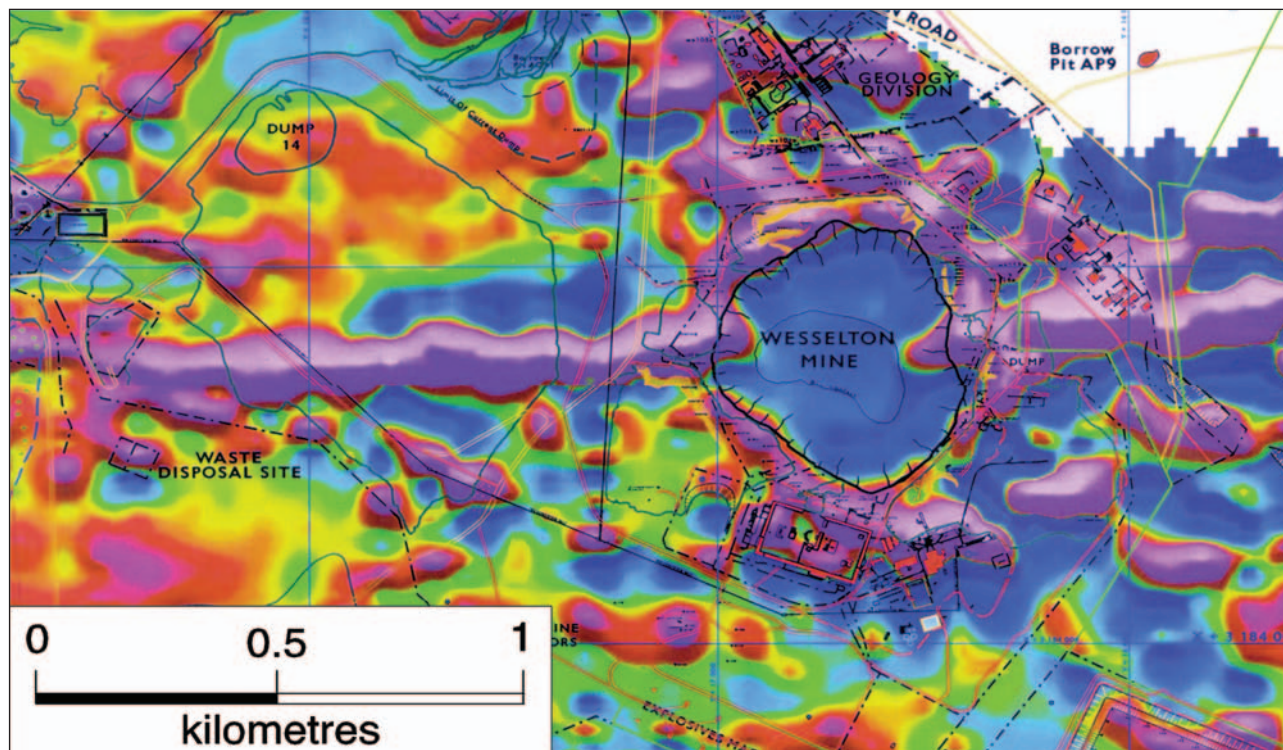
$$w^2 = 4\,kt \qquad (1)$$

where is the thermal diffusivity (= 5×10^{-7} m^2/s). For w = 1 to 5 cm the time scale is in the range 50 to 1000 seconds. If a 5 cm wide sill were emplaced over a representative distance of 500 m then the time scale must be considerably less than 1000 seconds, suggesting speeds of emplacement of several m s^{-1}. Sparks et al. (2006) estimated propagation speeds of 4 to 20 m s^{-1} for kimberlite magmas by applying a model of fluid-filled fracture propagation under turbulent flow conditions with high magma pressures (Lister and Kerr 1991).

Petrography
Analytical techniques
Thirty-two thin sections were examined. Sample locations are given in Figure 3. Mineral identifications were confirmed and textures studied using a Hitachi S-3500N scanning electron microscope with a 20kV accelerating voltage. Modal mineral proportions (Table 1) were determined using a combination of 2000 point count and image analysis of back-scattered SEM images for representative samples. Small-scale variations in modal mineral proportions were obtained by SEM image analysis on polished sections of two aphanitic samples (W1 and W2), one macrocrystic sample (W7) and one green aphanitic sample (E1). In total 46 images were captured using the SEM of which 43 were used for determining modal compositions using analySIS® 3.1 imaging software. Grey scale thresholds were set manually using image histograms for each sample prior to phase color coding and analysis of the images. Phases were identified as: serpentine as both pseudomorphs after olivine crystals and within the groundmass; calcite; phlogopite; perovskite and titanomagnetite/magnetite

Figure 7. *Visual representation of the results of the magnetic survey over Wesselton Mine. Note the linear purple feature (positive magnetic anomaly) that intersects the Wesselton pit and extends for 3 km in an east-west direction. The positive anomaly also extends 1 km radially around Wesselton pit, and to the northwest. Picture taken from an internal De Beers company report (2002).*

crystals and apatite as both crystals and within the groundmass. Six samples were selected for electron microprobe studies, two from each kimberlite variety. Silicate and carbonate minerals were analysed using a Cameca SX100 EPMA microprobe. Representative analyses are given in Tables 2 to 7 and the entire dataset can be accessed in a supplementary spreadsheet. We also refer to petrographic descriptions and mineral chemistry data on the macrocrystic sills and dykes from Shee (1985). Selected samples were analysed by XRD at the Natural History Museum, London to aid identification of alteration minerals.
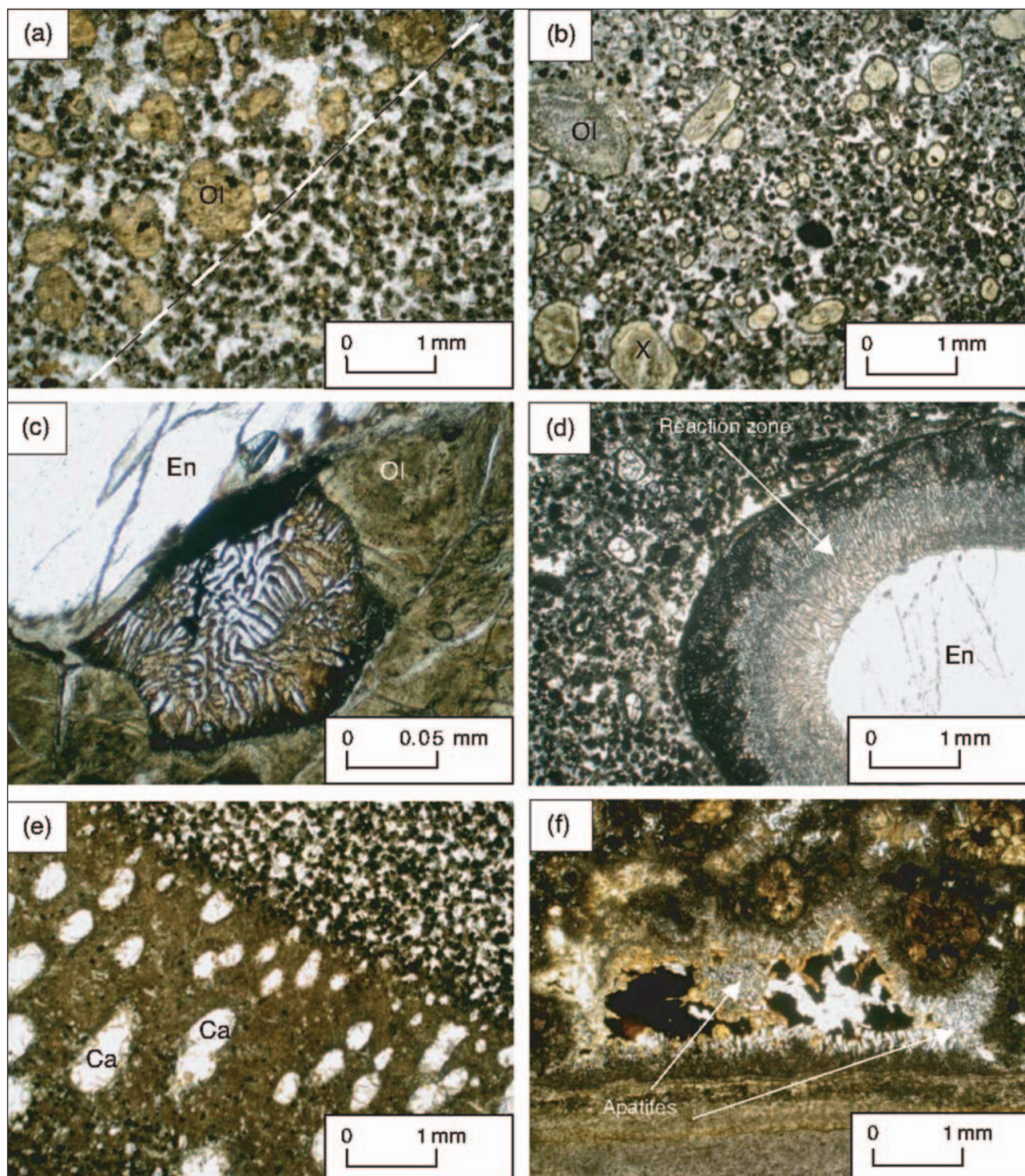
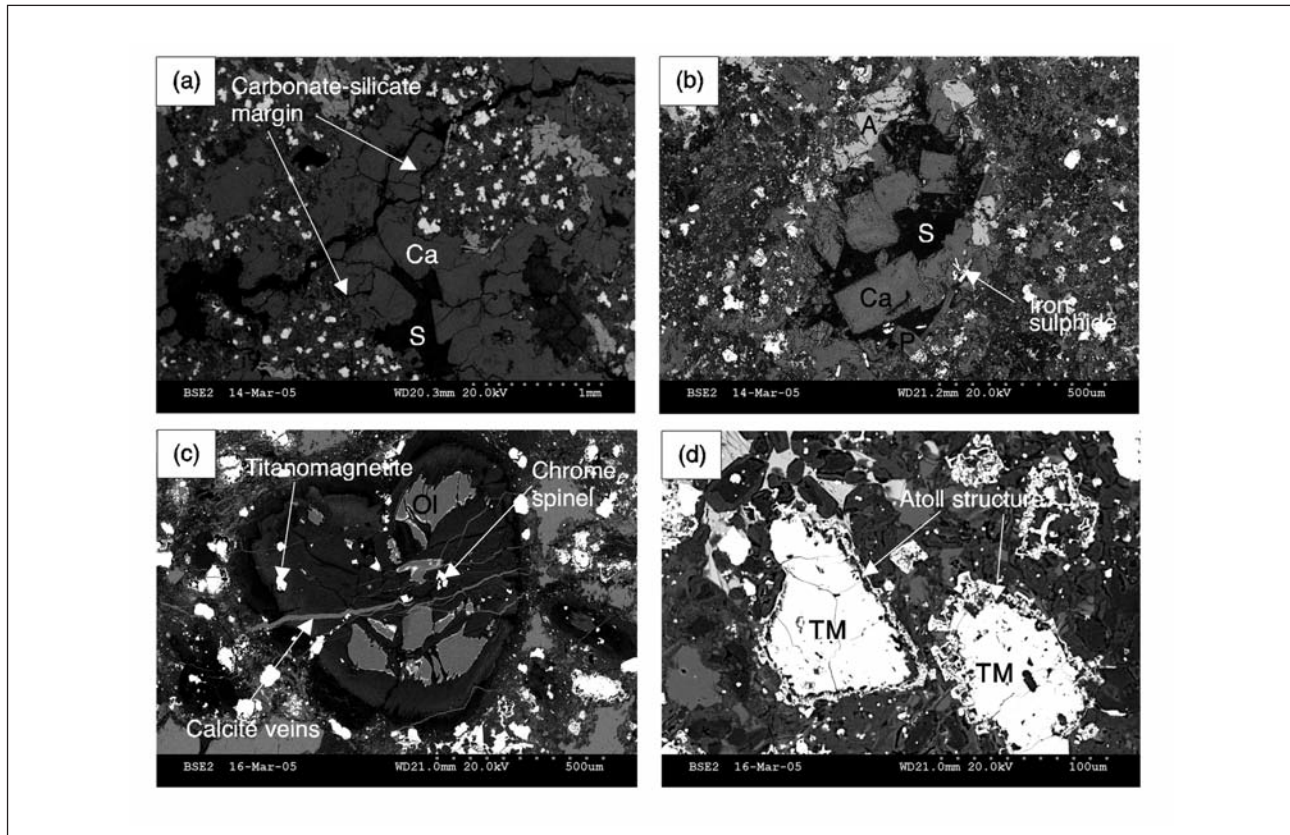## Petrography
Aphanitic kimberlite
Aphanitic kimberlite consists of serpentine, spinel, perovskite, barian phlogopite, calcite, smectite, apatite and rare ilmenite (Figure 8 and 9). Serpentine occurs as pseudomorphs of olivine microphenocrysts (0.05 to 0.2 mm) and disseminated in the groundmass. We did not find fresh olivine. Variations in modal data (Table 1 and Figure 10) reflect wide variations in mineral proportions on a thin-section scale. Grain size is variable, but many of the phases are in the 0.05 to 0.2 mm range with patches of very fine intimate calcite-phlogopite intergrowths. Olivine microphenocryst content (as pseudomorphs) varies from as much as 40% to absent (Table 1). The layered aphanitic rocks vary greatly in modal proportions on a thin-section scale (Figure 10a). Small-scale modal variations show that

olivine-rich areas are relatively rich in calcite and barian phlogopite, whereas olivine-poor areas are relatively rich in FeTi-rich spinel and perovskite (Figure 10b).
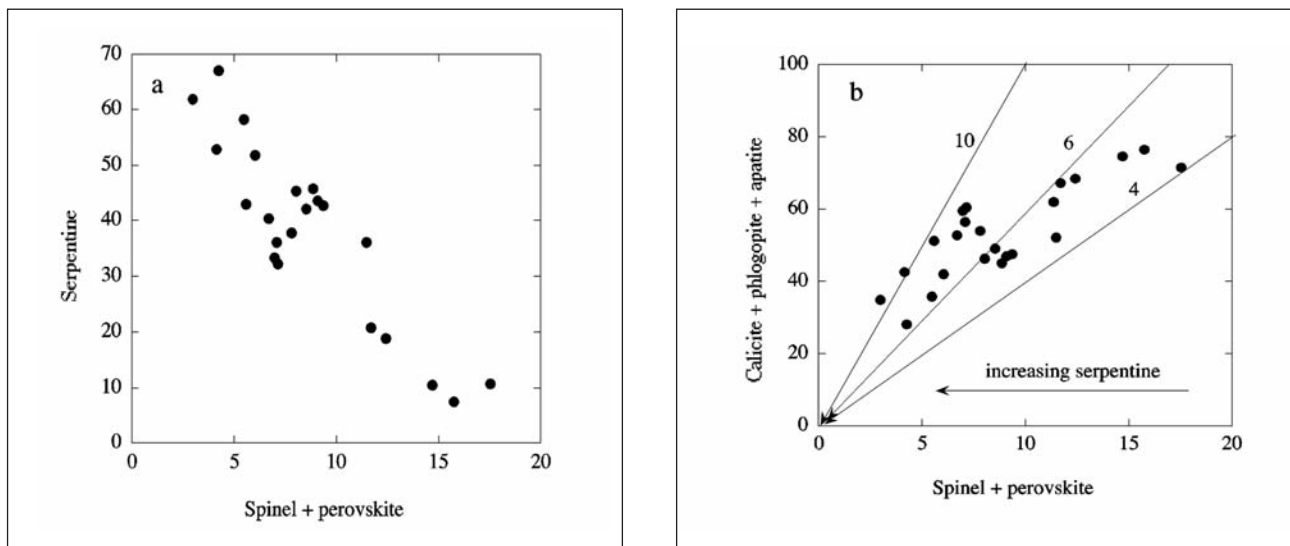
Serpentine associated with original olivine microphenocrysts shows textural zoning with an internal zone with a foliated texture and an outer zone with a structureless amorphous texture. The outer zone has an irregular complex boundary inter-grown with surrounding phases at the margins (Figure 11a). The inner zone has a ghost crystal shape and is interpreted as a pseudomorph of the original microphenocryst. The pseudomorphs commonly contain inclusions, including chrome spinel, FeTi-rich spinel, euhedral calcite and rare ilmenite (Figure 11a). The outer zone serpentine replaces matrix calcite and apatite, and euhedral phlogopite crystals are fretted at the contact with serpentine (Figure 11a). Perovskite and FeTi-rich spinel appear unaffected, although some perovskite crystal edges show minor embayment next to serpentine. There is also amorphous serpentine disseminated in the groundmass. The outer zone is interpreted as serpentine formed from the local release of excess chemical components from olivine during serpentinisation and replacing calcite and apatite. Disseminated serpentine has the same amorphous appearance as the outer zone of the pseudomorphs with irregular contacts with calcite; some of these serpentine patches may be the consequence of sectioning effects and related to an original olivine in the third dimension. For sample W2 we analysed 24 pseudomorphed olivine
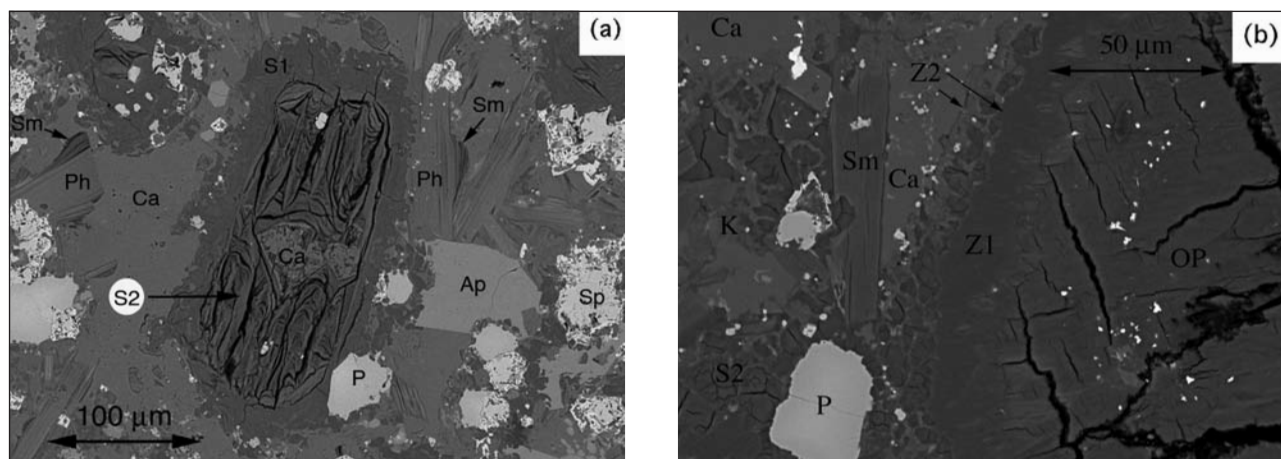
Figure 8. (**a**) *Two varieties of aphanitic kimberlite in the same sill (sample R6); the top half contains altered olivine microphenocrysts (Ol), the lower half does not (separated by a white dashed line). The darks minerals are spinel and perovskite, and the light interstitial areas consist of calcite, phlogopite and apatite. (**b**) Typical view of the macrocrystic kimberlite (sample P4). Note the difference between the euhedral olivine macrocrysts (Ol) and anhedral harzburgite microxenoliths (X), and the fine grained matrix. (**c**) Chromite and chrome diopside symplectite inside a harzburgite microxenolith (sample W7). The olivine (Ol) has been serpentinized, but the enstatite (En) remains unaltered. (**d**) Enstatite (En) xenocryst reacting with the kimberlite magma forming a four stage reaction rim (sample W7). See text for explanation. (**e**) The margin of Unit 3 (Figure 5), showing bounded carbonate globules (Ca) orientated normal to the margin in a fine grained serpentine rich chill-like zone (sample R6). (**f**) Micro-geode in the aphanitic kimberlite next to a lower shale layer (sample W2). Contains inwardly projecting apatite crystals with a centre of calcite and serpentine.*

Figure 9. *Backscattered electron images (**a**) Carbonate segregations in Unit 3 of Figure 5 containing calcite (Ca) and serpentine (S) (sample R6). (**b**) Carbonate-rich globule from the chill-like zone in Figure 5, containing euhedral calcite (Ca), serpentine (S), phlogopite (P) and apatite (sample R6). Note the coarse grained nature of the segregation compared with the groundmass. (**c**) Serpentinized olivine microphenocryst from the green aphanitic kimberlite (sample E1), exhibiting a fresh core (Ol), containing inclusions of chromite and titanomagnetite and thin calcite veins. (**d**) Titanomagnetite (TM) showing typical atoll structure present in all of the sill kimberlites (sample E1). The gap is filled with fine-grained serpentine and calcite. It was not possible to analyse the outermost spinel islands. Scale bar on each image.*

Figure 10. *(**a**) Modal percentages of serpentine versus [spinel + perovskite] to illustrate the local variability in the aphanitic sills (data from samples W1 and W2). (**b**) Modal variations of [calcite + phlogopite + apatite] plotted against [spinel + perovskite] in the aphanitic sills (data from samples W1 and W2). Lines of equal ratios of the two mineral groupings are shown to show that samples poor in serpentine (i.e. low original olivine content) are enriched in [spinel + perovskite] relative to [calcite + phlogopite + apatite].*
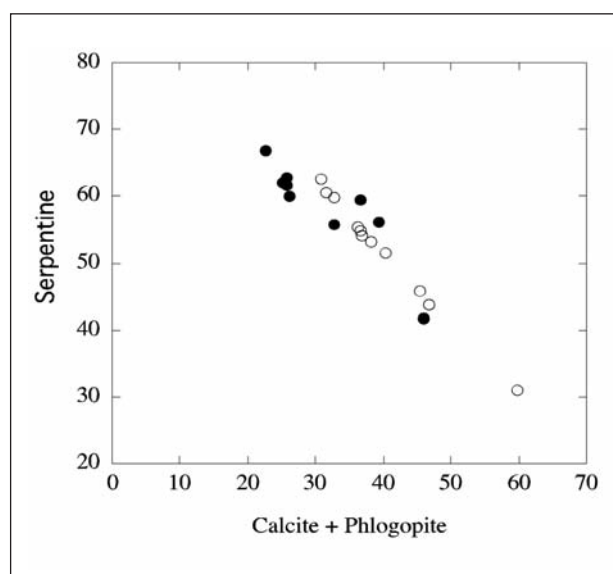
Figure 11. (**a**). *SEM image of olivine-bearing aphanitic sill. Serpentine in area S2 is interpreted as a pseudomorph after a euhedral olivine surrounded by a zone of amorphous serpentine that is replacing calcite (Ca), apatite (Ap) and phlogopite (Ph). Euhedral perovskite (P) and skeletal spinel (Sp) are unaffected by the serpentinisation. Note that the phlogopite crystals are replaced at the edges by smectite (Sm).* (**b**). *SEM image of a macrocryst pseudomorph (OP) after olivine and surrounding groundmass in macrocrystic sill (sample E7). The macrocryst is surrounded by two zones; an inner zone of amorphous serpentine (Z1) and an outer zone comprising a mixture of serpentine and "K-rich" serpiolite (marked by arrows). The surrounding groundmass consists of pseudomorphs of phlogopite replaced by smectite (Sm), calcite, and mixtures of disseminated serpentine (S2), perovskite (P), "K-rich" serpiolite (K) and fine-grained spinel (bright phase). The tiny bright minerals in the olivine interior are millerite.*

microcrysts distinguishing between the pseudomorphed core and the amorphous serpentine. From image analysis of sample W1 32% of the serpentine has the amorphous texture and 68% occurs as pseudomorphed cores (Table 1).

Compositions of serpentine (Table 3) are a predominantly FeO-rich (15 to 20%) and relatively MgO-poor (13 to 24%) variety. One sample contains a relatively MgO-rich (32 to 38%) variety. Qualitatively this suggests an iron-rich olivine precursor; if Mg/Fe ratios are conserved during alteration (as is the case in the other sills as described below) then estimated original olivine composition would have been about Fo_{60-70}. Serpentine groups minerals in kimberlites are commonly mixtures of different phases on a sub-micron scale (Berg, 1989; Stripp et al., 2006). We observed no magnetite, which is a common product of serpentinisation (Evans, 2004), but cannot exclude that the pseudomorphing material is a sub-micron scale mixture of Mg- end member serpentine and magnetite.
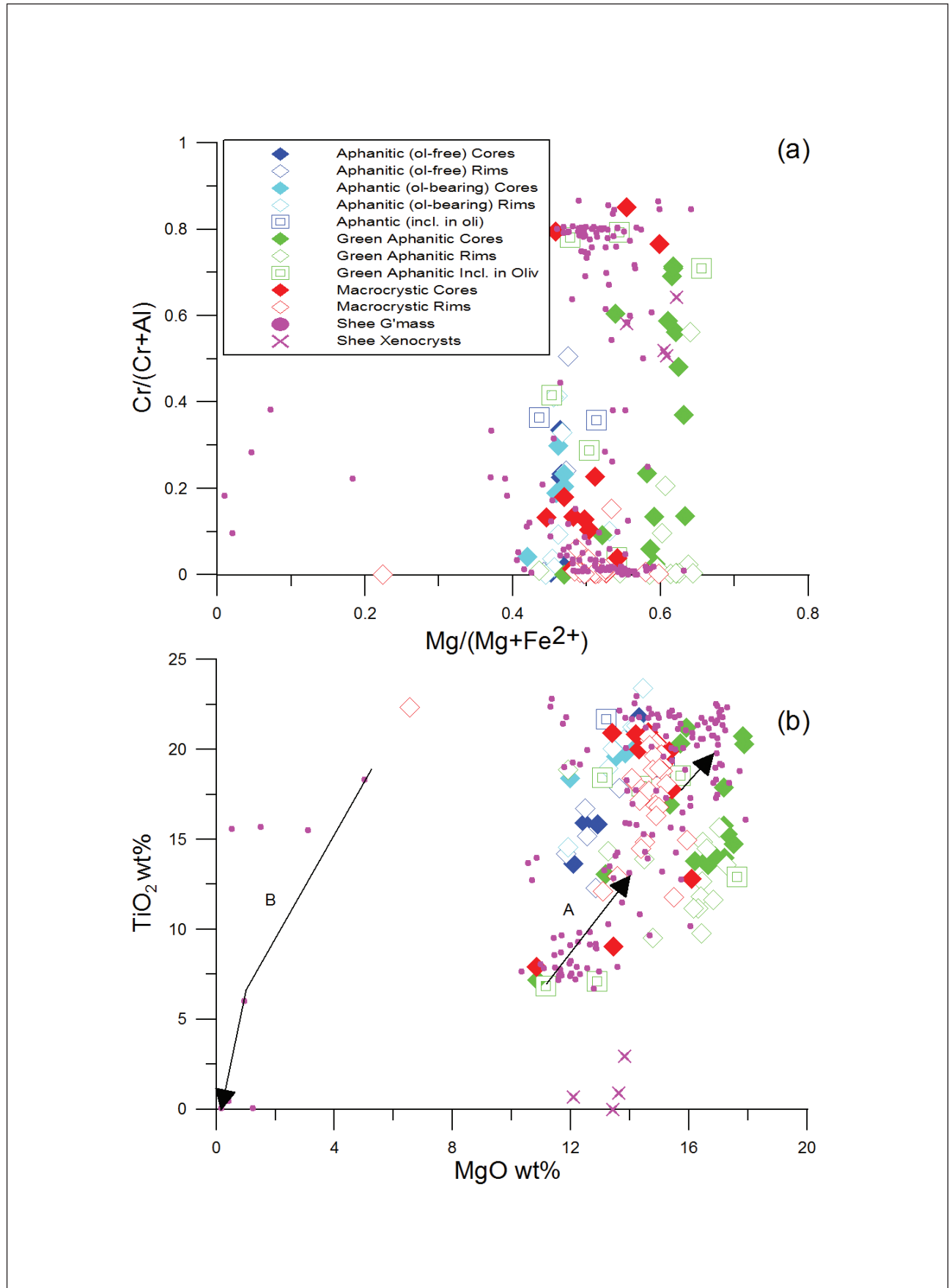
FeTi-rich spinel (up to 0.1 mm) displays homogeneous cores and skeletal margins (Figures 9a and 11a) with a Ti-rich alteration phase interpreted as leucoxene. Perovskite and apatite crystals are typically euhedral. Minor amounts of a clay mineral (smectite; see Table 5) partially or completely replace euhedral laths of phlogopite with splayed ends or textures suggestive of swelling (Figure 11a). Calcite forms a mosaic-like matrix between euhedral crystals, but itself forms euhedral crystals in coarse-grained patches. Phlogopite macrocrysts (up to 0.5 mm) show no preferred orientation and are commonly broken or kinked, indicative of deformation prior to incorporation into the kimberlite magma (Harris et al. 2004).

Figure 12. *Modal [serpentine+K-rich serpiolite] plotted against modal [calcite + phlogopite] for the macrocrystic kimberlite (E1: solid circles) and the green aphanitic kimberlite (W7: open circles). The negative correlation shows a spatial relationship interpreted as the consequence of replacement of calcite by serpentine in the immediate vicinity of olivine crystals.*

Macrocrystic kimberlite

This variety contains peridotite microxenoliths and olivine macrocrysts set in a matrix with an average grain size of 0.05 mm (Figure 8b). The groundmass is composed of varying amounts of olivine micro-phenocrysts, calcite, serpentine, apatite, phlogopite, saponite replacing phlogopite, a K–rich phase, spinel

Figure 13. *Mineral chemistry of spinels. (**a**) Cr/(Cr+Al) vesus Mg/(Mg +Fe^{2+}) and (**b**) TiO$_2$ versus MgO.Cr, Al Mg and Fe^{2+} are cation proportions calculated from the stiochiometry. Shee data refers to analyses from Shee et al., 1991.*

Figure 14. *Mineral chemistry of carbonates. (**a**) Plot of weight % FeO vs. weight % SrO. (b) Plot of weight % BaO vs. weight% SrO.*

Table 2.

1 to **3.** fresh olivine compositions from green aphanitic sill (sample E1);

4 to **7.** and from olivine xenocrysts in the macrocrystic sill (W7).

Further analyses of fresh olivine in Wesselton intrusions can be found in Shee (1985).

	1	2	3	4	5	6	7
SiO_2	39.14	39.76	39.13	38.86	38.82	39.44	39.55
FeO	13.43	13.53	13.35	13.24	13.10	13.26	13.15
MnO	0.17	0.17	0.16	0.13	0.14	0.14	0.16
MgO	46.84	46.33	45.94	47.31	46.87	46.79	46.50
CaO	0.15	0.09	0.11	0.05	0.06	0.06	0.06
NiO	0.18	0.34	0.21	0.30	0.30	0.32	0.22
Total	99.91	100.22	98.90	99.89	99.29	100.01	99.64

Table 3. Representative compositions of serpentine group minerals. No systematic compositional differences were found between serpentines replacing olivine and those in the groundmass.

1. Mg-rich serpentine in aphanitic sills;

2 to **4.** (samples W1 and W2) dominant Fe-rich serpentine in aphanitic sills;

5 to **7.** serpentine in green aphanitic sill (sample E1);

8 to **10.** serpentine in macrocrystic sills (sample W7).

88 analyses are listed in the supplementary data table.

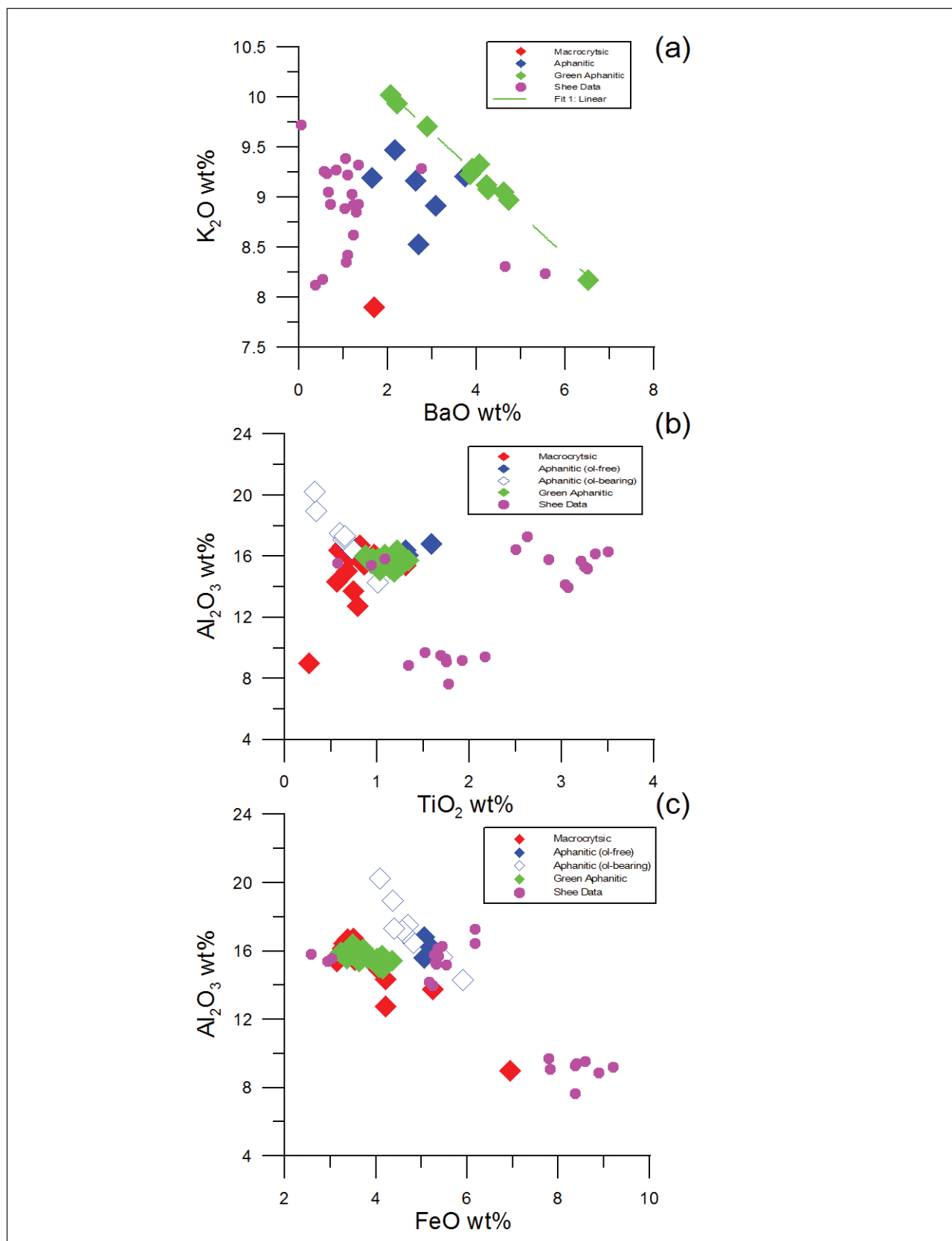|	1	2	3	4	5	6	7	8	9	10
SiO_2	40.53	44.63	40.86	41.23	41.84	38.15	35.71	38.32	40.66	42.15
Al_2O_3	0.88	1.21	2.19	0.95	0.63	0.99	2.19	0.18	0.51	0.67
FeO	6.33	17.49	15.78	20.61	6.97	11.06	13.93	12.42	6.22	7.89
MnO	0.08	0.16	0.34	0.2	0.11	0.18	0.22	0.4	0.15	0.2
MgO	38.17	17.93	21.38	18.9	36.89	34.62	32.93	32.69	37.15	34.39
CaO	0.13	1.07	0.91	0.94	0.03	1.5	0.07	0.15	0.15	0.41
Total	86.12	82.49	81.46	82.83	86.47	86.5	85.05	84.16	84.84	85.71

Table 4. Representative analyses of spinel and ilmenites.

1. ilmenite (aphanitic sample W2);

2. titanomagnetite-rim (macrocrystic sample W7);

3. titaniferous chromite-core (macrocrystic sample W7);

4. titanomagnetite inclusion in olivine (green aphanitic sample E1);

5. titaniferous chromite inclusion-core (green aphanitic sample E1).
*FeO calculated; Fe_2O_{3c} calculated, both using the method of Reed (1996). Mineral analyses undertaken using a microprobe with a beam diameter of 1μm, accelerating voltage of 20 kV, beam current of 10 nA, and count times of 10 s. Further 118 analyses of spinels and 5 ilmenites are listed in the supplementary data table.

	1	2	3	4	5
SiO_2	0	0.04	0.03	0.21	0.05
TiO_2	50.82	16.31	9.04	12.89	6.86
Al_2O_3	0.27	6.17	4.08	7.65	7.72
FeO	28.42	*11.87	*14.34	*7.25	*19.04
Fe_2O_{3c}	–	47.10	21.11	48.80	12.17
MnO	0.29	0.66	0.25	0.63	0
MgO	14.05	14.89	13.45	18.16	11.15
CaO	0.09	0.16	0.13	0.04	0
Cr_2O_3	4.90	0.12	34.79	1.63	41.01
NiO	0.04	0.11	0.09	0.21	0.20
Total	98.88	97.43	97.31	97.47	98.20

(chrome spinel zoned to FeTi-rich rims) with minor perovskite, rare ilmenite and millerite (Table 1 and Figure 11b). Shee (1985) describes abundant monticellite as a major constituent of the groundmass of some macrocrystic sills and dykes (up to 44%), but noted that monticellite was absent from samples containing abundant calcite and phlogopite. We did not observe monitcellite in our samples, which are of the calcite-phlogopite variety. The K-rich phase contains principally K (~10 weight % K_2O), Mg and Si with minor Fe but no Al. XRD analysis established the presence of abundant serpiolite, and we interpret the K-rich phase as serpiolite with abundant K within molecular channels; the K is released by alteration of phlogopite to saponite. Olivine macrocrysts are partially to completely replaced by high-birefrigent serpentine and some have inclusions of chrome spinel, perovskite and FeTi-rich spinel.

Serpentinised olivines have Mg/Fe ratios consistent with preserving the original Mg/Fe of the original olivines. XRD analysis confirmed the serpentine polytype as lizardite. The pseudomorphed olivines are texturally zoned with prominent polygonal partings in the pseudomorphed interior (Figure 11b) and margins consisting of an inner zone of structureless serpentine and an outer zone of polygonally textured serpentine intimately intergrown with the K-rich serpiolite (Figure 11b). Tiny inclusions of NiS (probably millerite) occur in the core of the serpentised

Figure 15. *Mineral chemistry of phlogopites. (**a**) Plot of K_2O versus BaO for the Wesselton phlogopites. The line is a linear regression through the phlogopite data (r^2 value = 0.993) in the green apahnitic sill. The line passes through the pure phlogopite and kinoshitalite end members, indicating that these phlogopites have not been altered. (**b**) Plot of Al_2O_3 versus TiO_2 and (**c**) Al_2O_3 versus FeO. Shee data refers to analyses Shee (1985) and Shee et al., (1991), and are from three samples of macrocrystic sills and dykes.*

Table 5. Representative carbonate compositions:

1 to **3.** groundmass calcites in aphanitic sills;

4 to **5.** (samples W1 and W2), groundmass calcite in green aphanitic sill (sample E1);

6. calcite inclusion in olivine (sample E7);

7 to **8.** groundmass calcite (macrocrystic sample W7);

9. hydrothermal calcite vein.

70 analyses are listed in the supplementary data table.

	1	2	3	4	5	6	7	8	9
MgO	nd	nd	0.01	0.01	nd	0.20	<0.01	0	5.31
CaO	55.74	57.36	56.46	56.77	57.05	55.49	56.99	56.44	48.95
FeO	0.05	0.18	0.18	0.07	nd	1.73	0.03	0.09	0
SrO	1.86	1.28	0.72	0.14	0.53	nd	0.36	0.70	0.07
MnO	0.02	nd	0.01	0.01	<0.01	0.03	nd	0	0.03
BaO	0.05	nd	nd	0.06	0.05	0.01	0.02	0.20	0
Total	57.72	58.89	57.38	57.06	57.64	57.46	57.41	57.45	54.38

Table 6. Representative phlogopite compositions:

1 to **3.** aphanitic sills (samples W1 and W2);

4 to **6.** green aphanitic sill (sample E1);

7. macrocrystic sill (sample W7).

There are 83 analyses in the supplementary table, 30 of which have BaO data. There are 12 analyses of phologopites from macrocrystic sills and dykes with BaO data in Shee (1985).

	1	2	3	4	5	6	7
SiO_2	35.94	36.20	36.40	36.57	35.69	33.94	36.91
TiO_2	0.29	1.09	0.36	0.73	0.89	0.92	1.21
Al_2O_3	17.87	16.72	17.26	15.47	15.55	16.29	12.11
FeO	4.72	5.40	4.92	4.02	4.14	3.88	6.84
MnO	0.07	0.10	0.08	0.06	0.04	0.05	0.29
MgO	23.15	22.87	23.24	24.21	23.37	23.28	24.60
CaO	0.40	0.28	0.25	nd	0.12	0.04	0.19
Na_2O	0.01	0.05	0.07	0.01	0.02	0.09	0.51
K_2O	9.20	9.21	9.47	10.02	9.33	8.17	7.90
BaO	1.64	3.73	2.15	2.06	4.06	6.51	1.70
Total	93.29	95.65	94.20	93.14	93.21	93.17	92.26

macrocrysts, but are absent from the marginal zones (Figure 11b). An abundant high-birefrigent serpentine forms irregular patches in the groundmass, commonly with a mixture of polygonal textured serpentine mixed with the K-rich serpiolite surrounding a core of structureless serpentine (Figure 11b).

Serpentine appears to replace igneous calcite; a negative correlation between modal calcite and serpentine plus the K-rich serpiolite is consistent with this interpretation (Figure 12). Euhedral phlogopite is commonly partially or completely replaced by saponite (Figure 11b, Table 5 and identified by XRD). Some altered samples have coarse patches of calcite and low-birefringent serpentine (serpophite); in some cases well-shaped calcite crystals and pools of serpophite suggest a void-filling texture. Serpentine compositions (Table 3) are rich in MgO compared to those in the aphanitic sills and are near end member lizardite compositions.

Harzburgite microxenoliths are composed of olivine, enstatite and symplectites of chromite and chrome diopside (Figure 8c). Discrete rounded grains of enstatite

also occur and are derived from fragmented peridotite xenoliths (Figure 8d). The harzburgites contain chromite and chrome diopside symplectites, with NiS (millerite) inclusions (Figure 8c). Enstatite macrocrysts are commonly mantled by a reaction rim, containing four zones (Figure 8d). The innermost zone, zone 1, contains tiny (0.05 mm) elongate anthophyllite crystals in a matrix of phlogopite; zone 2 contains anthophyllite crystals in a matrix of chrome diopside (0.7 to 2% Cr_2O_3); zone 3 contains elongate anthophyllites in a matrix of phlogopite, and zone 4 is an oxide rich layer (Figure 8d). Shee (1985) describes reaction rims around orthopyroxene of fine serpentised olivine, phlogopite, spinel and possible glass in other Wesselton rocks.

Green aphanitic kimberlite

This rock is composed of serpentinised olivine microphenocrysts with rare fresh remnants, calcite, dispersed serpentine, FeTi-rich spinel, perovskite and varying amounts of phlogopite and apatite (Table 1). Compositions of serpentine replacing olivine are consistent with preservation of the original Mg/Fe ratios

Table 7. Representative compositions of saponite clay replacing phlogopite in the macrocrystic sill (sample W7). na= not analysed.

	1	2	3	4	5	6
SiO_2	27.83	27.68	29.49	30.90	32.19	26.82
TiO_2	1.02	1.39	1.59	1.94	1.67	1.57
Al_2O_3	21.34	19.94	20.95	17.02	22.96	19.45
FeO	4.9	5.74	3.8	7.75	4.51	6.89
MnO	0.17	0.12	0.1	0.15	0.08	0.30
MgO	21.14	24.8	22.68	24.84	24.53	24.44
CaO	0.66	2.27	2.86	1.57	2.28	0.95
Na_2O	1.71	2.59	1.13	1.61	1.45	3.26
K_2O	2.13	0.84	0.36	0.94	0.27	2.23
BaO	na	na	na	0.38	1.18	2.83
Total	80.9	85.37	82.96	87.10	91.12	88.74

of the replaced olivines. Disseminated serpentine replacing calcite is observed in zones surrounding olivine pseudomorphs. Chrome spinels, FeTi-rich spinels, perovskite, calcite, barytes and rare ilmenite inclusions occur in altered olivines. Secondary calcite veining is abundant. Phlogopite and apatite occur with globular concretions of barytes at the margins of the calcite veins, indicating that the veining is hydrothermal.

Classification
The Wesselton intrusions classify as calcite kimberlites within the nomenclature of Mitchell (1986; 1995). Some of the calcite-rich aphanitic rocks classify as carbonatites based on the proposed 30% calcite threshold proposed by Mitchell (2005) and within the IUGS scheme based on modal mineralogy (Le Maitre, 2002).

Textures
Layering. The aphanitic varieties are composite and exhibit prominent layering due to alternations in the presence and absence of olivines. Figure 5 shows three different layers in one thin section. Unit 1, the marginal phase, has no chilled margin next to the shale and is characterised by olivine pseudomorphs (Figure 8a). The olivine pseudomorphs are not observed directly adjacent to the shale contact. Unit 2 contains elongate patches of Unit 1, suggesting that Unit 2 intruded into Unit 1. Unit 2 is finer grained than Unit 1 and olivine pseudomorphs are rare or absent. Phlogopite is concentrated in bands or discrete areas in the matrix. The contact of Unit 3 exhibits a very fine grained, serpentine-rich, chilled margin containing phlogopite, apatite, calcite and rare opaques (Figure 5). This zone contains elongate patches of carbonate orientated normal to the contact (Figure 8e). Towards the centre of Unit 3 there is a transition to a coarser well-developed segregation texture, which separates carbonate-rich areas from silicate-oxide-rich areas (Figure 5 and 9a).

Carbonate-rich segregations
The chilled margin of Unit 3 in the aphanitic kimberlite contains oval-shaped, carbonate-rich, bounded segregations, 0.01 to 1.8 mm in size (Figures 8e and 5). These segregations contain an interlocking mass of

carbonate, with varying proportions of apatite, phlogopite, serpentine and rare iron sulphides (Figure 9b). The phlogopite crystals grow from the margin towards the centre. These segregations are relatively coarse grained compared with the surrounding groundmass (Figure 9a and 9b).The larger segregations (towards the centre of Unit 3) are composed of interlocking calcite and apatite (Figure 9a).

Glomerocrysts (crystal clusters)
The olivine microphenocrysts in the aphanitic kimberlite occasionally show glomeroporphyritic texture with local clustering of several olivine pseudomorphs. Perovskite and spinels commonly form a 'necklace' around the olivine aggregates. Spinels and perovskites in the matrix typically form clusters of 3 to 4 grains. Large spinel and perovskite crystals are commonly surrounded by several smaller grains of the same minerals.

Micro-geodes
The aphanitic sill contains inwardly growing apatite crystals with a carbonate, serpentine and iron hydroxide centre (Figure 8f). The apatite crystals are projecting into a void. Thin veins of carbonate and serpentine run along the shale contact, with apatite crystals orientated normal to the contact (Figure 8f).
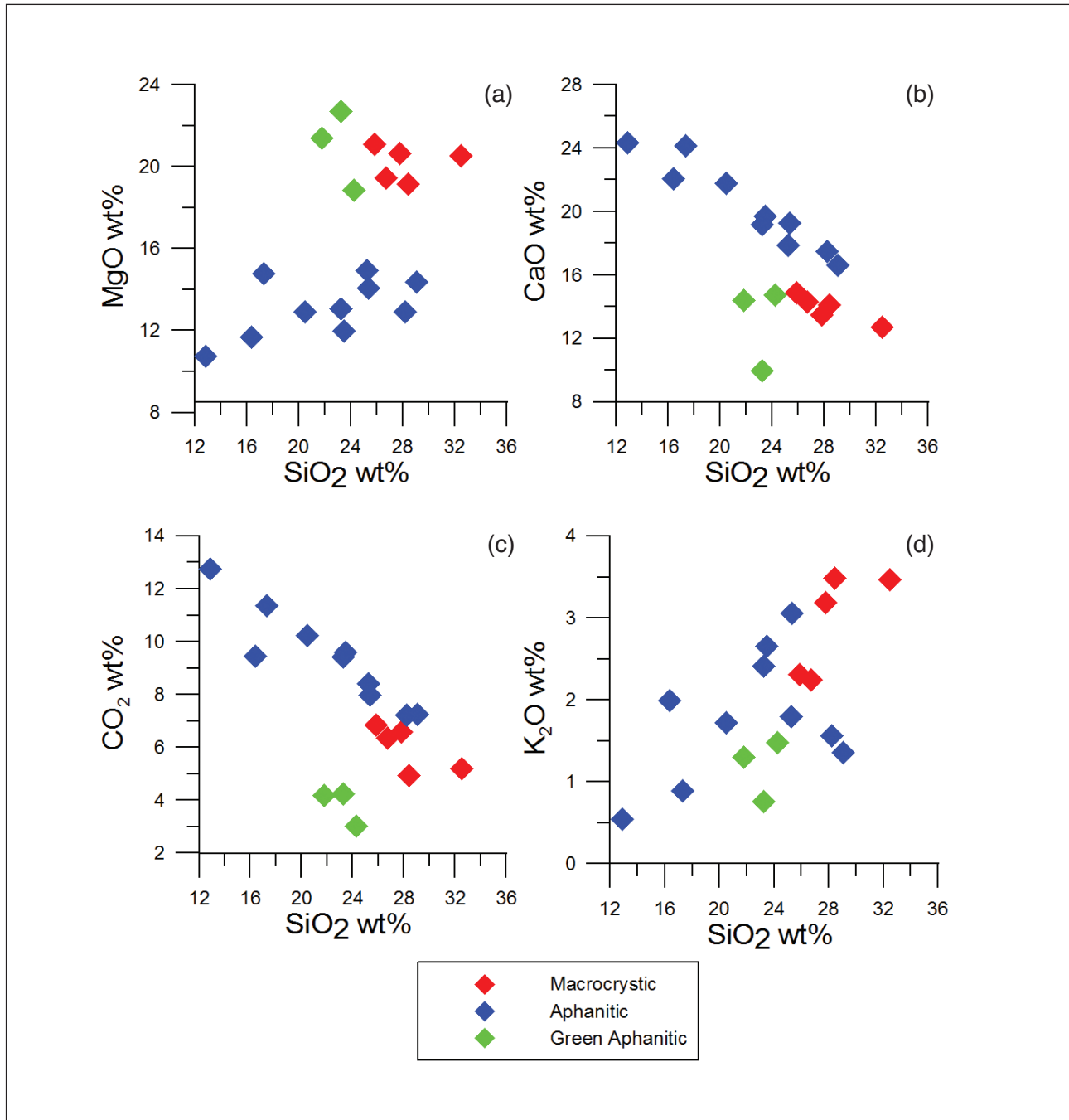
Mineral chemistry
Olivine
Olivine occurs as microphenocrysts, macrocrysts and xenocrysts (Table 2). Rare fresh macrocrysts of olivine in our samples had ~Fo_{86} Fresh olivine remnants in microphenocrysts in the green aphanitic kimberlite have Fo_{84-87} (Figure 9c and Table 2). Shee (1985) reported two populations of olivine, namely those with typical mantle compositions (Fo_{90-93} and NiO 0.35 to 0.4 weight %) of likely xenocrystal origin and those with more Fe-rich compositions (Fo_{83-87} and NiO 0.05 to 0.35 weight %) of likely phenocrystal origin.

Serpentine
Serpentinized olivines in the macrocrystic the green aphanitic sills have FeO/(FeO + MgO) in the range 0.14 to 0.38 and 0.16 to 0.31 respectively. Those in the

Figure 16. (*a*) *Variations of MgO* (*b*), *CaO* (*c*), *CO$_2$* (*d*) *and K$_2$O with SiO$_2$ for the Wesselton kimberlite sills and dykes.*

aphanitic sills overlap in FeO/(FeO + MgO) but several have FeO/(MgO + FeO) between 0.4 to 0.52. It seems that the serpentine compositions reflect the FeO contents of the original olivine crystals. Serpentine (Table 3) from pseudomorphs of olivine micro-phenocrysts and macrocrysts contain low Al$_2$O$_3$ contents with a mean of 1 weight %, 1.8 weight % and 0.5 weight % for the aphanitic, green aphanitic and macrocrystic sill olivine pseudomorphs respectively. Despite pronounced textural differences (Figure 10 and 12), the marginal zones and interiors of olivine pseudomorphs have indistinguishable compositions.

Spinel
Spinels occur as groundmass crystals, inclusions in olivine microphenocrysts and 'necklaces' around earlier crystallising spinels and olivine pseudomorphs (Table 4). The groundmass spinels commonly form atoll-like structures where the core and rim are separated by a gap of fine-grained serpentine and calcite (Figure 9d). The groundmass spinels predominantly consist of solid solutions of the end-members ulvospinel, magnesioferrite and spinel (sensu stricto). Spinel compositions, including data from Shee (1985), are displayed in terms of Cr/(Cr + Al) versus Mg number

(Figure 13a) and TiO$_2$ versus MgO (Figure 13b). The data indicate that each sill type shows distinct compositional fields, notably reflected in Mg number and MgO, and strong fractionation trends, such as wide variation of Cr/(Cr + Al) and increasing TiO$_2$ with increasing MgO. The green aphanitic sill has notably high Mg number, reflecting the more primitive character of the magma. There are spinel inclusions in olivine and a small number of groundmass spinels from the green aphanitic sill with compositions similar to the spinels found in the aphanitic and macrocrystic sills. These data suggest that the green aphanitic sill is younger than the other sills. We also note that the spinels sampled by Shee et al., (1991) overlap with our data but form high and low TiO$_2$ clusters, one of which overlaps with our data, but the other falls in separate field.

Ilmenite
Ilmenite occurs as discrete crystals commonly mantled by FeTi-rich spinel and as inclusions inside olivine phenocrysts (Table 4 and supplementary data table). MgO values are in the range 10.9 to 16.5%. Most have Cr$_2$O$_3$ in the 2 to 5.5 weight % range. We follow Shee (1985) in interpreting the Cr-rich compositions as evidence that ilmenite forms before the groundmass spinel, which would be expected to incorporate Cr preferentially if co-precipitated with ilmenite. For two cases of ilmenite inclusions in fresh olivine we calculated temperatures using the thermometer of Anderson and Lindsley (1979). For the green aphanitic sill with ilmenite (Gk$_{55.9}$ Il$_{40.7}$ Hm$_{4.0}$) and olivine (Fo$_{85}$) the calculated temperature is 1100°C. For the macrocrystic sill, using data from Shee (1985) with ilmenite (Gk$_{51.8}$ Il$_{40.7}$ Hm$_{7.5}$) and olivine (Fo$_{86}$), the calculated temperature is 930°C. The temperatures are only weakly dependent on pressure: the estimates would be approximately 20°C higher at 13 kbars. Anderson and Lindsey (1979) estimate errors of 20 to 30°C, but the effect of chromite solid solution is unknown. The higher temperature estimate for the green aphanitic sill is consistent with the higher Mg number of groundmass spinels.

Carbonate
Carbonates occur in the groundmass, carbonate segregations, secondary veining and replacement pseudomorphs inside olivine pseudomorphs (Table 5). MgO contents are low in the secondary veining (<6 weight %) and very low in the primary groundmass calcite (< 0.01 weight %). Groundmass calcite in the aphanitic sills contains high Sr contents (1.9 weight % SrO), compared with 0.7 weight % and 0.3 weight % SrO in the groundmass of the macrocrystic and green aphanitic sills respectively (Figure 14a). BaO contents are generally below about 0.07 weight % (Figure 14b), but have higher values in groundmass calcite from the macrocrystic sill (up to 0.2 weight %). Calcite that replaces olivine has very low SrO and elevated iron

contents (up to 1.80 weight % FeO), compared with 0.1 weight % FeO in the groundmass of the same sample (Figure 14a). This feature suggests the calcites replacing olivine phenocrysts inherit their high FeO content from the olivine. Secondary vein calcites divide into those with very low SrO and those with low SrO (Figure 14a).

Groundmass calcite is considered a primary igneous phase rather than a product of secondary alteration because:
1. calcite poikilitically encloses and is intergrown with other igneous minerals;
2. high Sr calcites are consistent with crystallisation from a high temperature melt rich in trace elements (Armstrong et al. 2004);
3. flow aligned apatites are preserved in calcite segregations; and
4. the late stage hydrothermal calcite veins have different compositions, notably negligible Sr and Ba (Table 5).

Phlogopite
Phlogopite chemistry is summarised in Figure 15, including data in Table 6 and from Shee et al. (1991). The green aphanitic sill has Barium-rich phologopite which falls on the expected solid solution line from end member K-phlogopite to kinoshitalite (Figure 15a), indicating up to 25% of the kinoshitalite end member. Data on K-Ba in the aphanitic and macrocrystic intrusions are less coherent than the green aphanitic kimberlite, falling below the ideal solid solution line (Figure 15), suggesting incipient alteration. The Mg, Al and Fe data indicate solid solution with the theoretical eastonite mica end member in the field of aluminous phlogopite. These compositions are typical of groundmass phlogopite in Group 1 kimberlites (Mitchell 1995). Like the spinels pholopites fall into several distinct fields in terms of FeO, Al$_2$O$_3$ and TiO$_2$ (Figure 15b and 15c). There is little overlap between our data and those of Shee et al. (1991) which show two well-defined clusters of high and low TiO$_2$ compositions. This observations further highlights individuals sills have different compositions as reflected in mineral chemistry and that our study broadens the recorded diversity. Shee (1985) reports 0.3 to 0.9 weight % fluorine in the Wesselton phlogopites, noting that we did not analyse for F.

Saponite
We have recognised two clay mineral phases that partly (Figure 11a) or completely (Figure 11b) replace phlogopite with prominent swelling textures (Figure 11a). Probe data (Table 7) give low totals (82-91%), high Al$_2$O$_3$ and low K$_2$O in comparison to phlogopite (Table 5). XRD of whole rocks powders show saponite as a major constituent with swelling properties. The probe data show significant amounts of BaO, reflecting the composition of the original phlogopite.

Table 8. Bulk-rock major and trace element analyses of hypabyssal kimberlite from the Wesselton sill complex. **1** to **6.** macrocrystic sill (1, sample D2; 2, sample P1; 3, sample P4; 4, sample W7; 5, sample W9; 6. W10); **7** to **15.** aphanitic sill (7, sample W2; 8, sample J1; 9, sample J4; 10, sample J3; 11, sample R1; 12, sample R2; 13, sample R3; 14, sample R4; 15, sample R6); **16** to **18.** green aphanitic sill (16, sample K2; 17, sample E1; 18, sample K1). Major and minor element compositions quoted in wt.% and ppm respectively. $Fe_2O_3^T$ total iron as Fe_2O_3. Mg# is defined as the molar ratio of MgO to (MgO + FeO).

	1	2	3	4	5	6	7	8	9	10	11	12	13	14	15	16	17	18
SiO_2	32.49	28.42	27.79	26.72	25.84	25.33	16.37	17.30	12.85	20.47	23.46	29.05	28.21	25.24	23.23	21.78	23.23	24.25
TiO_2	2.84	4.22	3.45	3.50	3.69	4.92	9.20	6.57	8.00	8.45	9.42	7.54	9.48	6.54	9.00	5.10	9.59	7.35
$Al_2O_{3_T}$	2.33	3.93	2.85	2.65	2.78	2.80	3.90	2.55	4.52	3.38	3.91	2.69	3.43	2.69	2.77	4.61	3.18	3.37
Fe_2O_3	10.95	13.54	14.59	15.31	13.48	14.14	16.77	14.35	15.41	12.33	12.62	12.90	11.79	14.77	15.01	14.73	16.80	14.85
MnO	0.21	0.26	0.25	0.28	0.25	0.27	0.26	0.25	0.25	0.26	0.27	0.22	0.28	0.25	0.27	0.26	0.29	0.22
MgO	20.53	19.16	20.63	19.44	21.09	14.07	11.67	14.76	10.75	12.92	11.97	14.38	12.91	14.93	13.08	21.37	22.71	18.84
CaO	12.73	14.11	13.47	14.32	14.86	19.27	22.05	24.12	24.33	21.79	19.70	16.62	17.47	17.86	19.19	14.41	9.94	14.75
Na_2O	0.52	0.23	0.17	0.38	0.16	0.55	0.38	0.02	1.21	0.22	0.56	1.00	1.30	0.39	0.47	0.02	0.19	0.00
K_2O	3.47	3.49	3.19	2.24	2.31	3.06	1.99	0.89	0.55	1.72	2.65	1.36	1.56	1.80	2.41	1.30	0.76	1.48
P_2O_5	1.90	1.85	1.23	2.04	1.94	3.42	2.55	1.98	1.41	2.86	1.87	1.54	1.20	2.23	1.86	4.85	0.69	6.29
LOI	11.42	10.36	12.06	12.13	12.81	11.45	13.79	16.76	18.78	15.28	13.74	12.80	12.63	12.88	12.79	10.42	12.53	8.30
CO_2	5.21	4.95	6.60	6.34	6.86	7.99	9.46	11.37	12.76	10.23	9.61	7.26	7.22	8.40	9.42	4.18	4.25	3.04
SO_2	0.63	0.11	0.82	0.24	0.72	1.37	0.15	0.14	0.19	0.49	0.93	0.35	2.64	1.08	2.36	0.50	0.27	0.76
H_2O	5.58	5.30	4.64	5.55	5.23	2.09	4.19	5.25	5.84	4.56	3.21	5.19	2.76	3.40	1.00	5.74	8.01	5.50
Mg#	78.8	73.7	73.7	71.5	75.5	66.3	55.3	67.0	57.9	67.6	65.3	68.9	64.7	66.7	63.3	70.3	72.8	71.5
Total	99.38	99.58	99.68	99.00	99.21	99.28	98.93	99.54	98.07	99.68	100.17	100.09	100.26	99.57	100.08	98.85	99.92	99.68
V	260	110	115	180	224	312	326	323	303	253	150	140	113	168	128	279	0	200
Cr	1068	1345	1366	1685	1504	891	704	870	899	871	677	782	941	804	837	841	1142	764
Co	54	63	63	68	64	65	72	70	71	72	62	70	66	77	75	67	81	72
Ni	590	468	533	605	630	303	137	301	262	314	201	354	333	372	300	291	350	257
Cu	47	37	46	85	72	105	87	85	40	115	80	57	45	81	74	170	31	290
Zn	98	109	114	125	117	133	142	127	141	127	136	111	121	107	118	118	112	112
Ga	9	12	11	10	9	15	17	15	18	13	16	13	21	10	13	14	14	13
Rb	123	86	90	86	113	139	122	60	38	128	136	84	79	98	112	106	43	142
Sr	1645	1704	1451	2202	2022	2149	2512	1990	1991	1922	1833	1301	1175	1619	1674	2097	1039	2686
Y	39	49	46	46	41	42	49	45	47	41	50	39	47	40	38	45	42	37
Zr	439	1399	856	347	328	651	706	558	687	720	589	411	375	597	429	803	541	847
Nb	298	510	428	378	335	338	438	351	418	363	397	321	352	325	354	389	357	440
Mo	1.7	2.1	0.6	0.0	1.1	1.5	0.0	0.7	2.4	1.2	0.0	5.3	2.0	0.0	0.0	1.4	0.0	0.0
Ba	2136	543	1418	1391	2618	2066	7098	1260	11247	2073	1109	555	637	887	1072	4540	564	4515
La	203	270	255	239	219	169	207	178	238	–	–	–	–	–	194	–	–	–
Ce	296	396	394	393	346	259	258	300	302	–	–	–	–	–	285	–	–	–
Nd	114	142	148	146	131	101	114	119	139	–	–	–	–	–	113	–	–	–
Pb	13	18	9	13	13	19	12	18	7	18	10	9	4	5	7	13	8	14
Th	32	33	34	44	38	26	35	31	29	21	25	19	25	20	27	29	28	17
U	7.2	7.8	3.4	6.6	0.9	4.6	6.9	3.8	4.1	10.6	8.0	7.6	5.5	5.2	9.7	4.4	11.7	9.8

Table 9. Estimates of kimberlite compositions compared with Wesselton aphanitic sills.

Compositions normalised to 100% free of the volatile constituents (H_2O and CO_2) to facilitate comparison. The volatile constituents are also reported. Values in wt.%.

1. average composition of fine-grained groundmass around autoliths in Lesotho kimberlites (Ferguson et al., 1975);

2. average of 6 compositions of kimberlite collected from the aphanitic margins of the Jericho Pipe, Canada (Price et al., 2000);

3. indicative melt composition deduced from compositions of aphanitic intrusions, Kimberley by Le Roex et al. (2003), noting that composition has been slightly modified from the published estimate following personal communication from A. Le Roex;

4. primary melt composition for the Uintjiesberg kimberlite, South Africa (Harris et al., 2004);

5. estimate of kimberlite melt composition based on secondary melt inclusions (Golovin et al., 2003);

6. Composite sample of Benfontein kimberlite (Hawthorne 1968);

7. most silica-rich olivine-bearing aphanitic sill from Wesselton sill complex (sample D2);

8. most SiO_2 poor olivine-poor aphanitic sill from Wesselton sill complex (sample W2).

	1	2	3	4	5	6	7	8
SiO_2	33.60	35.66	32.73	29.56	34.35	27.90	33.64	16.21
TiO_2	3.76	0.76	1.82	3.82	1.79	2.09	8.73	10.01
Al_2O_3	3.34	1.83	2.67	2.74	2.82	3.18	3.12	5.70
FeO	14.05	7.97	10.90	11.24	9.80	12.39	13.82	19.43
MnO	0.31	0.19	–	0.22	0.18	0.24	0.25	0.31
MgO	24.80	29.35	32.73	30.80	36.88	32.89	16.66	13.55
CaO	16.14	22.46	14.55	17.73	12.45	15.05	19.24	30.68
Na_2O	0.29	0.37	–	0.07	0.35	0.01	1.16	1.53
K_2O	1.96	0.54	2.42	1.35	0.92	0.17	1.58	0.69
P_2O_5	1.48	0.87	2.18	2.21	0.46	2.44	1.55	1.78
Cr_2O_3	0.27	nd	–	0.26	–	–	–	–
CO_2	7.00	13.02	7.00	8.63	6.9	3.28	5.21	6.46
H_2O+	7.44	6.68	8.00	4.92	–	7.39	5.59	4.19

K-rich serpiolite

This phase has the morphology of a sheet silicate (Figure 11b) and has been identified by XRD. It contains 9 to 11% K_2O, 20 to 24% MgO, 40% SiO_2, 10 to 12% FeO and 1 to 2% Al_2O_3. It has only been identified in the macrocrystic sill.

Calcium zirconate (2.7 to 4.8 weight % TiO_2), titanian kimzeyite (11.9 to 13.5 weight % TiO_2) and hollandite (69.9 to 72.2 weight % TiO_2) have previously been reported in the Wesselton sills by Mitchell (1991).

Bulk rock geochemistry

18 samples of hypabyssal kimberlite from the Wesselton sill complex were analysed for major and trace elements using XRF techniques at Leicester University. The data are reported in Table 8. In addition Shee (1985) in his Tables 7.2 and 7.3 presented major element, Ni and Cr data on three macrocrystic sills and two of aphanitic sills; these data are included here.

Major element geochemistry

There are clear geochemical differences between the aphanitic, macrocrystic and green aphanitic samples (Table 8), notably the SiO_2, TiO_2, MgO, CaO, K_2O and CO_2 contents. MgO and SiO_2 show a broad positive correlation for the aphanitic sills, and the macrocrystic and green aphanitic intrusions have much higher MgO contents reflecting the high abundance of serpentine and original olivine (Figure 16a). The olivine-poor and olivine absent aphanitic sills have low SiO_2 contents (<20 to 12.85%). A macrocrystic dyke (sample D2) has the highest MgO and SiO_2 values; an aphanitic dyke has the lowest (sample J4), and the green aphanitic kimberlite contains comparable MgO but lower SiO_2 than the macrocrystic samples. There are well-defined negative correlations of SiO_2 with CaO (Figure 16b) and CO_2 (Figure 16c) for the aphanitic and macrocrystic sills, largely reflecting variations in igneous calcite content. There is a scattered trend of increasing K_2O with increasing SiO_2 (Figure 16d) with the macrocrystic rocks showing some of highest K_2O contents. The three intrusion groups are separated on a plot of MgO versus TiO_2 (Figure 17). Other major elements are generally poorly correlated.

The olivine-bearing aphanitic sills share the characteristics of low SiO_2 (~25 to 30 %), low Al_2O_3, low Na_2O and moderate K_2O with other examples of aphanitic hypabyssal intrusions and reconstructions of Group 1 kimberlite compositions (Table 9). Note that none of the compositions in Table 9 are likely to
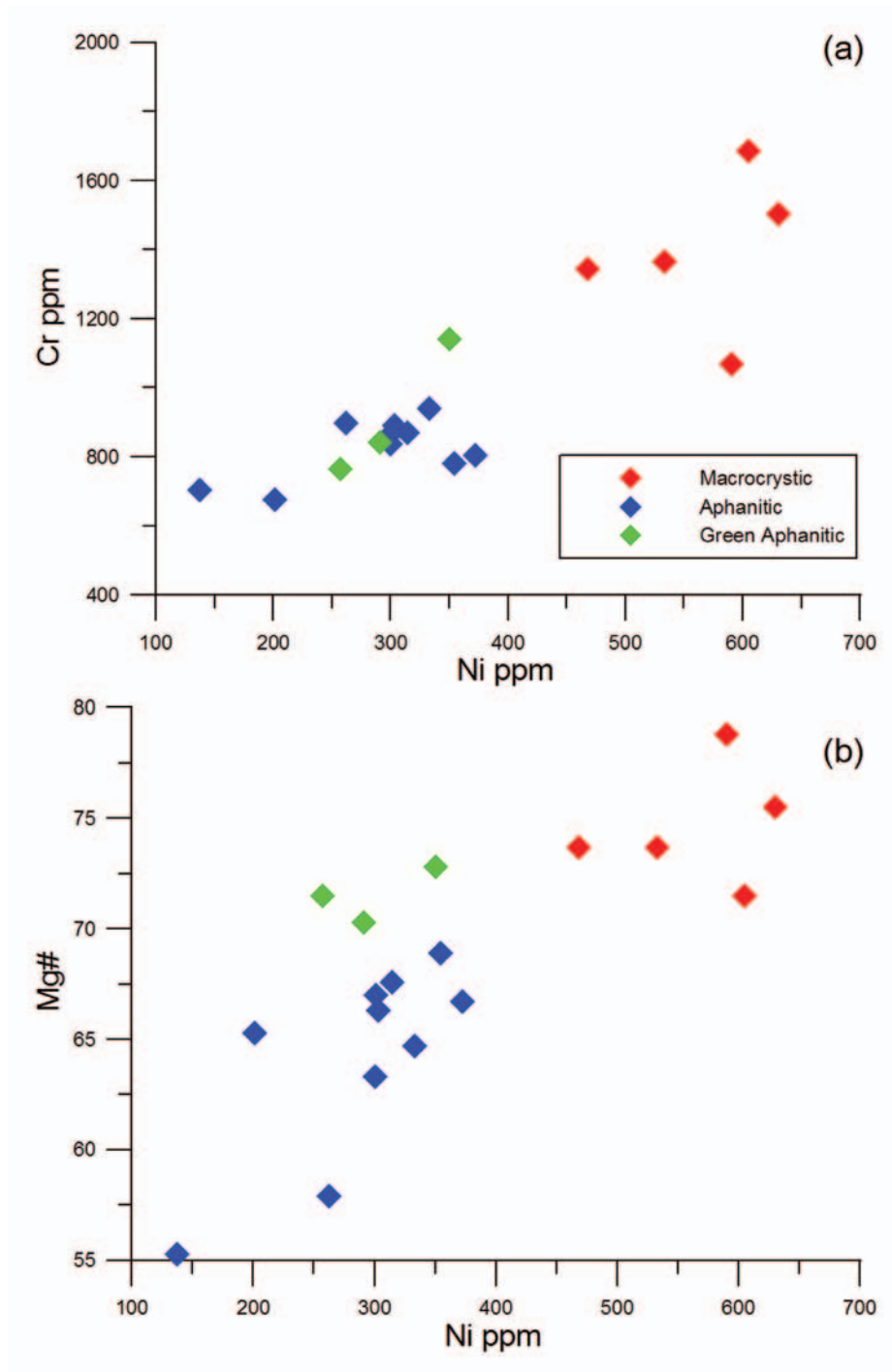
Figure 17. *Variations of MgO and TiO₂ for the Wesselton sills and dykes.*

Figure 18. *Co-variation of Nb with Ni in Wesselton kimberlite sills and dykes.*

Figure 19. *Co-variations of Cr (**a**) and Mg# (**b**) with Ni in Wesselton kimberlite sills and dykes.*

represent true kimberlite melts, because of the major effects of serpentinisation on bulk compositions (Sparks et al., 2009). The Wesselton sills have significantly lower MgO contents and TiO_2 contents two to three times higher than these other estimates. The aphanitic sills tend towards carbonatite compositions and have distinctively high CaO and TiO_2 contents. Sills associated with carbonatitic groundmasses and segregations are known from the nearby Benfontein sills in the Kimberley district (Dawson and Hawthorne, 1973) and in the Mela sill, Archangelsk region, Russia (Beard et al., 2000). Carbonatite segregations in the Mela sill are similar in composition, but have low TiO_2 content and even lower SiO_2 contents.

Trace element geochemistry

Trace element concentrations are highly variable (Table 8) and most show non-systematic variations. Cr and Ni show a good positive correlation with the aphanitic sills being depleted in these elements relative to the macrocrystic and green aphanitic intrusions (Figure 19a). Ni shows a positive correlation with Mg# with three groups being discriminated (Figure 19b). Ni increases from 137 ppm in an aphanitic sill to 800 ppm in a macrocrystic sill with increasing Mg# from 55 to 79. This reflects changes in modal olivine abundance. The high field strength elements (HFSE) and light rare earth elements (LREE) show high and variable abundances (Zr 328 to 1400 ppm; Nb 298 to 510 ppm; La 169 to 269 ppm). Within the aphanitic rocks there is a negative linear relationship between Nb and MgO, reflecting considerable variation within this sill. A plot of Ni versus Nb (Figure 18) shows different negative linear relationships for each of the main sills. This may reflect modal abundance variations of olivine (Ni) and perovskite (Nb), but may also reflect geochemical uniqueness or evolution of each sill. Th (17-38 ppm) is higher in the macrocrystic rocks. The large ion lithophile elements (LILE) are also high and variable in abundance (Rb 38 to 141 ppm; Ba 543 to 11247 ppm; Sr 1038 to 2686 ppm; Pb 4.2 to 19.5 ppm).

Petrogenesis

Inferring the compositions of kimberlite magmas and their petrogenesis are considerable challenges as consequence of their polybaric history, tendency to entrain and assimilate mantle and crustal materials during magma ascent, and almost ubiquitous alteration. As recognised by previous workers (e.g. Dawson and Hawthorne, 1973; Mitchell, 1986; Price et al., 2000; Le Roex et al., 2003; Harris et al., 2004; Becker and Le Roex, 2006; Mitchell, 2008) aphanitic intrusions represent the most promising material to study. We consider in reverse order the main processes that have affected the petrogenesis of the Wesselton sills, namely: partial melting of the deep mantle; assimilation and crystallization during magma ascent; high-level crystal differentiation just prior to or during sill emplacement; degassing; and low temperature alteration. Each of these

largely sequential processes has left its imprint on the petrological and geochemical characteristics.

Alteration

The dominant alteration process in the Wesselton intrusions is serpentinisation of olivine. A ubiquitous feature is that olivine crystal pseudomorphs can be distinguished from surrounding zones of amorphous serpentine (Figure 11). The texture implies that groundmass phases, notably igneous calcite and apatite, have been replaced by serpentine, implying an open chemical system in which components such as Ca and CO_2 have removed by a fluid phase. This interpretation is supported by the correlation between the ratio of replaced to resistant phases (Figure 12) and serpentine content. Serpentinisation involves large volume changes and pseudomorph textures require the release of up to 40% of the original mass of the olivine (Evans, 2004; Stripp et al., 2006; Sparks et al., 2009) as well as the addition of large volumes of water. The ratio of serpentine in olivine pseudomorphs to the amorphous serpentine of 2:1 is consistent with this hypothesis. In a hypabyssal rock with limited porosity, the excess volume must either be removed from the system or must replace unstable phases. The style of alteration in the Wesselton sills has major implications for assessing the primary compositions of kimberlites. CaO and CO_2 are removed in a chemically open system and consequently SiO_2 and MgO are relatively enriched in the remaining rock. The changes are more pronounced as the olivine content increases and much of the original igneous groundmass calcite can be removed. Barian phlogopite can be partly replaced by serpentine (Figure 11a), shows evidence of incipient alteration from Ba and K data in some samples (Figure 15), and is commonly partly or completely replaced by saponite (Figure 11). In the macrocrystic sill K has been redistributed to form K-bearing serpiolite intergrown with serpentine.

Serpentinisation reactions can take place from low ambient temperatures (Kelly et al., 2005) to temperatures up to about 500°C. The very short cooling times of the sills make serpentinisation during their cooling unlikely. However, the adjacent Wesselton kimberlite pipe might have heated the intrusions and generated hydrothermal systems that provided favourable ambient conditions for alteration. Deuteric alteration from magmatic volatiles may also have contributed to alteration.

Many of the trace elements and some major elements are highly variable with non-systematic trends e.g. Ba. We attribute these characteristics to open-system alteration with many of the phases that contain normally incompatible trace elements, such as calcite, barian phologopite and apatite being unstable in the fluids associated with alteration. Recent observations of warm springs at the Lost City site (Kelly et al., 2005) confirms the highly alkaline, reduced character of the serpentising fluids and the transport of Mg, Ca, Si and (CO_3^{2-}) in solution to form brucite and aragonite chimneys on the

sea floor as a consequence of reaction with host rock minerals in the mantle. Such open-system behaviour is also anticipated in alteration of kimberlites. We note that open system serpentinisation of kimberlite leads to them having compositions that cannot form from low temperature igneous melts as discussed in more detail by Sparks et al. (2009).

Syn-emplacement processes

Igneous layering documented at the Benfontein sills has been interpreted as the result of numerous injections of small amounts of kimberlite magma that consolidated in thin tabular sheets (Dawson and Hawthorne, 1973). Many of the layers show magmatic sedimentation features, implying in situ differentiation due to crystal-melt separation, which was taken as evidence that the magma was emplaced as a hot and mobile fluid (Dawson and Hawthorne, 1973). The aphanitic Wesselton sills display thin multiple layers with olivine-rich and olivine-absent varieties (Figure 5) and thin-section scale heterogeneities. Pre-injection differentiation of olivine may have occurred resulting in olivine-bearing and olivine-absent varieties (Figure 5). The olivine-rich layers have a glomeroporphyritic texture, which can form by:

1. entrainment of crystal mushes from a pre-existing cumulate (Jerram et al., 2003);
2. sticking together by either settling or flow (i.e. like synneusis) (Schwindinger, 1999); or
3. heterogeneous nucleation (Jerram et al., 2003).

It is unlikely that the olivines clustered in situ because the thin sills cooled very quickly and show quench textures. Olivine crystals are not found directly adjacent to the shale contact, suggesting flow and wall effects were important. This is consistent with olivine crystallization prior to or during emplacement into the sills. The olivines may have been concentrated away from the sill margins by flow differentiation (Komar, 1972). Separation of olivine and melt prior to and in the early stages of intrusion can account for these observations.

The proportions of FeTi spinel and perovskite increase relative to calcite, phlogopite and apatite as olivine content decreases in the aphanitic sills (Figure 10). These variations are mirrored in the major element variations. This observation indicates that the compositional spectrum is not only controlled by olivine addition or removal; the surrounding groundmass, presumed to represent a melt, must change composition systematically as olivine content varies. In addition the evidence from discrete trends and compositional clusters in spinel and phlogopite mineral chemistry indicates several different geochemical distinct magma batches were emplaced into the sill complex. It is unclear whether these variations are caused by differentiation of the melts prior to crystallization or a physical sorting of the phases during crystallization and emplacement.

The origin of the bounded calcite segregations is controversial. Previous studies have considered the segregations to be immiscible liquids (Clement, 1975; Clarke and Mitchell, 1975; Beard et al., 2000), or alternatively amygdales formed by vesicles that were breached and filled with residual carbonate-rich fluid (Donaldson and Reid, 1982). Mitchell (1984) argued that the lack of textural evidence for open space filling or breaching of the margins of the segregations suggests that they were formed by the separation of an immiscible residual carbonate-rich liquid. However, the presence of abundant igneous calcite in the surrounding fine matrix argues against true liquid immiscibility. As an alternative we suggest that the segregations were produced by either vapour-melt immiscibility in a mesostasis, or by late stage residual melt segregations. The coarse grained nature of the segregations show an analogy to drusy cavities, which precipitate out minerals from the vapour phase that are in equilibrium with the crystals and residual melt (Henderson, 1970).

Chrome spinels, FeTi-rich spinel and ilmenites occur as inclusions in the olivines suggesting that they are primary grains that crystallised contemporaneously with the olivine phenocrysts (Shee et al., 1991). The spinel inclusions and groundmass spinels show a similar evolution, from a chrome-rich core to a titanomagnetite rim, typical of other hypabyssal kimberlites (e.g. Benfontein; McMahon and Haggerty, 1984)).

The occurrence of phlogopite in the sills and dykes implies that water was present, as well as abundant CO_2. The complex reaction rims around the enstatite xenocrysts show that it is not a stable phase and the presence of anthophyllite and ubiquitous phlogopite in the reaction zone suggests that the kimberlite magma is hydrous. In contrast the Benfontein kimberlite sills and Igwisi kimberlite lava flow, which are also carbonate rich, contain negligible amounts of phlogopite (Dawson and Hawthorne, 1973; McMahon and Haggerty, 1984; Dawson, 1994).

The kimberlite-carbonatite connection

The Wesselton sills show a wide range in composition (e.g. 12 to 29 weight % SiO_2) from olivine-bearing to olivine-absent varieties rich in igneous calcite. Some calcite-rich rocks classify as carbonatites by both the criteria of IUGS (Le Maitre, 2002) and Mitchell (2005); even more would be carbonatite when the replacement of igneous calcite by serpentine (Figure 11) is taken into account. The rock types are intimately related in composite and layered sills, supporting the formation of carbonatites in close association with kimberlite. Several lines of evidence support this:

1. the abundance of primary calcite;
2. presence of apatite and high titanium magnetite (Bailey and Kearns, 2002);
3. high Sr and La contents (Dawson and Hawthorne, 1973); and
4. high concentration of incompatible elements (Gudfinnsson and Presnall, 2005).

Figures 16c and 16d show the strong variations of CO_2 with CaO with SiO_2 in the Wesselton rocks, which

reflect the continuous variation of relative proportions of calcite and serpentine after olivine. Mitchell (2005) prefers the term calcite kimberlite for these rocks to emphasize that the calcite-rich rocks are not genetically related to the carbonatites associated with nephelinites and melilitites. However, these and other kimberlite-associated calcite-rich rocks (see Mitchell, 2005) are transitional to a variety of carbonatite magma.

Evidence for distinct unrelated magma batches

Our data indicate that the Wesselton sills complex involves multiple intrusion of several magma batches with contrasts in the inventory of suspended olivine crystals and distinct melts compositions as reflected in groundmass mineral compositions and evolutionary trend, being most prominent in spinels (Figure 14) and phlogopites (Figure 15). There is also evidence of mixing between these batches from spinel inclusions in olivine crystals and mixed populations of spinels. This is also reflected in distinct Nb versus Ni trends (Figure 18).

We now consider the relationship between the aphanitic rocks and the macrocrystic rocks. One possibility is that the former is derived from the latter by physical removal of the harzburgite and olivine macrocrysts from the melt (e.g. Harris et al., 2004; Le Roex et al., 2003). For example, stalling of macrocrystic magma at depth could allow the settling of the suspended crystals and xenoliths through the low viscosity melt; then the ascent of the melts to form the aphanitic magmas. Data on TiO_2 (a component resistant to alteration) provide difficulties for this hypothesis. The TiO_2 contents of the macrocrystic sills are less than half of the aphanitic sills (Table 8), requiring at least 50% of olivine and xenolith removal. However, modal data suggest that the typical content of suspended xenoliths and macrocrysts is insufficient to generate a melt with the observed high TiO_2 in the aphanitic rocks. Removing harzburgite from the macrocrystic samples to give to the most silica-poor aphanitic samples is also impossible because the MgO value generated is much lower than is observed.

An alternative interpretation is that the aphanitic magmas are related to the macrocrystic magmas by the former incorporating mantle during ascent followed by partial dissolution of olivine and reaction with orthopyroxene to generate the macrocrystic magmas. This process can readily occur in ascent of kimberlite magmas from great depth because the adiabat of volatile under-saturated melts is less than the decrease of the melt liquidus temperature with decreasing pressure (Kavanagh and Sparks, 2009). Thus the melts become superheated as they ascend and therefore able to assimilate entrained mantle silicates. The melt composition in the macrocrystic magma is thereby altered to a more TiO_2-poor melt by the dilution effect. This model could account for the TiO_2 problem, but not the higher K_2O in the macrocrystic magmas. The addition of harzburgite to the most silica-poor aphanitic sample generates an MgO value much higher than is observed in the silica-rich aphanitic sample.

The data are therefore inconsistent with a model of fractionation alone, or mantle assimilation alone, to produce the observed variation in magma batch mineralogy and chemistry. The close proximity of several different geochemically and mineralogically distinct magma batches to one another and the variable incompatible element concentrations (e.g. Ti, K) is consistent with an origin in a heterogeneous mantle from stockwork metasomatism (Bailey, 1984).

Fractionation, assimilation or partial melting?

The nature of kimberlite magmas and the controlling igneous processes remain enigmatic (Mitchell, 2008; Sparks et al., 2009). Interpretations of deep igneous processes are confounded by the alteration, presence of xenocrysts and xenoliths, by possible physical sorting of crystals according to size and density and by the difficulty of interpreting the origin of the olivine component (Brett et al., 2009).

The low Ni, Cr and Mg#, and the high TiO_2 content of the aphanitic sills (and to a lesser degree, of the green aphanitic sill) are consistent with removal of olivine and chrome spinel either by fractionation or by separation of melt from xenocrysts. Variations in the modal proportions of olivine account for much of the diversity in these sills and the carbonate-rich, olivine-absent rocks can be explained by olivine fractionation. The lack of both xenocrystal and phenocrystal components in the aphanitic sills also points to fractionation and stalling of the intrusion en route to surface. The abundant xenocrysts and xenoliths in the macrocrystic sill are observations that are hard to reconcile with fractionation. However, the mantle xenocrysts in the Wesselton sills appear to be derived from the shallow mantle in the spinel lherzolite field (Shee et al., 1991). Therefore fractionation at greater depths prior to incorporation of the xencrysts could explain the geochemical variety.

Interpretation is complicated by two additional factors. Firstly, variations in petrological characteristics can also be attributed to variations in the source composition of a veined, heterogeneous and metasomatised carbonated mantle (e.g. Bailey, 1984; Shee et al., 1991). Features that can be interpreted by crystal fractionation can also be interpreted by partial melting processes.

Secondly, kimberlite magma compositions are affected by the assimilation of mantle and crustal components during ascent. There is direct evidence for these processes having taken place in the macrocrystic rocks with rounded xenocrystal olivine and strong reaction textures around orthopyroxenes derived from the mantle xenoliths. This is a manifestation of a more general observation of the scarcity of orthopyroxene xenocrysts in kimberlites, even though harzburgite and lherzolite xenoliths are commonly abundant (Mitchell, 1986). Assimilation of orthopyroxene can be explained by its instability in highly unstable in hydrous, melts (Edgar and Chabonneau, 1993; Shee, 1985; Mitchell,

2008). Assimilation of orthopyroxene xenocrysts during ascent should have the following consequences. The melts would become enriched in SiO_2 and MgO and depleted in incompatible elements (such as TiO_2 and K_2O) and evolve away from carbonatite compositions. The enrichment in SiO_2 and MgO would also promote crystallization of olivine (e.g. Otto and Wyllie, 1993).

Physical and thermodynamic constraints

Kavanagh and Sparks (2009) presented numerical calculations of kimberlite ascent taking into account decompression of the melt, exsolution of volatiles, physical entrainment of xenoliths, assimilation and olivine crystallization. Magmas generated from the asthenosphere (e.g. Dasgupta and Hirschmann, 2006) or base to the lithosphere (e.g. Bailey, 1984; Dalton and Presnell, 1998) are unlikely to reach the Earth's surface without major changes arising from decompression and mechanical, thermal and chemical interactions with the surrounding mantle.

The models of Kavanagh and Sparks (2009) indicate typical cooling's of 150 to 300°C with substantial olivine crystallization at low pressure. Starting temperatures are constrained by geotherms inferred from studies of mantle xenoliths at temperatures of around 1350 to 1450°C (Priestley et al., 2006). The temperatures of 1100°C from olivine-ilmenite compositions in the relatively primitive green aphanitic magma and the estimates of 1030 to 1170°C by Fedortchouk and Canil (2004) for Lac de Gras kimberlites are thus consistent with these model results. The lower temperature estimate of 930°C calculated for the macrocrystic dyke at Wesselton can be explained by physical entrainment of mantle xenoliths during ascent, which increases the cooling substantially. The aphanitic Wesselton kimberlites represent residual and fractionated carbonate-rich melts separated from early formed phenocrysts and entrained xenoliths prior to be being emplaced.

Conclusions

The excellent exposure of the Wesselton sill complex provides a unique opportunity to study precursor hypabyssal kimberlite activity in the Kimberley area. The main conclusions are summarised below:

1. The sill complex is composed of multiple injections of petrographically and geochemically distinct kimberlite magma that intrude the upper Dwyka shales immediately below a Karoo dolerite sill. Three major groups of hypabyssal kimberlite are identified: (a) aphanitic kimberlite with variations from rocks rich in olivine microphenocrysts to rocks with little or no olivine; (b) macrocrystic kimberlite containing entrained harzburgite microxenoliths; and, (c) 'green' aphanitic kimberlite. The aphanitic magmas were followed by intrusion of the macrocrystic magmas. The green aphanitic sill is the youngest because it contains some xenocrysts derived from the macrocystic and aphanitic sills. Variations in the mineral chemistry of spinels and phlogopites in the aphanitic sills suggest that this group is itself made up of several discrete magma batches.

2. Emplacement of the sill complex was governed by the rigidity of the dolerite sill, which prevented the magma from breaching the surface, the morphology of the host rock and the local and regional crustal stress systems. Pre-existing weaknesses (e.g. shale bedding) provide an easy path for sill intrusion, but local variations in sill orientations suggest early intrusions distorted the local stress field, a consequence of a multi-episode event. Feeder dykes and joints predominantly strike east to west and northwest to southeast and imply a regional stress field with the principal vector of compression in the horizontal planes between east-west and northwest to southeast, a trend that can be recognised all the way to Lesotho.

3. The thin sills and absence of internal chills indicates very fast emplacement of very low viscosity magma. Speeds of several m s^{-1} are estimated based on thermal time scales and models of the propagation of magma-filled fractures under turbulent flow conditions. The high magma pressures with magmatic pooling and pressure build-up below the dolerite sill implied by the small and large scale structures of the sill complex lend support to the kimberlite emplacement model discussed by Field and Scott Smith (1999), although the actual trigger for initial volcanic explosions and the downward growth of the pipe is not known.

4. Like many kimberlites serpentine is a major component of the Wesselton intrusions. Although some kimberlite researchers assert that the serpentine has an igneous origin (e.g. Mitchell, 2008), alteration by external fluids in a chemically open system is much more consistent with the evidence. We have demonstrated replacement textures of igneous groundmass minerals by serpentine derived from altered olivine in rocks of low porosity. The textures also show that replacement has taken place after groundmass crystallization in situ. The very large increase in volume that occurs in serpentinisation requires the system to be open with selective removal of some components, here notably Ca and CO_2, and relative enrichment in others, notably MgO and SiO_2. Open system serpentinisation changes the bulk composition of the rocks significantly with the affects being most pronounced for olivine-rich varieties. Such open system alteration processes are the paradigm for formation of serpentine in any other igneous rock except for kimberlites. Further problems with viewing serpentine as having an igneous origin are discussed in Sparks et al. (2009).

5. The aphanitic kimberlite range from olivine-bearing to olivine-absent varieties with carbonatitic affinities.

These kimberlites have undergone crystal-liquid separation prior to or during incorporation into the sills, resulting in internal sill layering and variable compositions. These low viscosity, hydrous carbonate-rich magmas formed bounded carbonate segregations, micro-geoids and clusters of olivine phenocrysts due to flow.

6. On the basis of geochemical data and mineral assemblages, the different magma batches cannot be related to one another by any simple igneous processes. The macrocrystic variety shows evidence of reaction between orthopyroxene and kimberlite melt. When emplaced in the shallow crust, the melt compositions are transitional to carbonatite melts. The magmas have been affected by both silica-enrichment processes (orthopyroxene assimilation) and by silica-depletion processes (olivine crystallization) during magma ascent and emplacement. The sills are unlikely to record the original melt compositions generated in the deep mantle source region.

7. Kimberlites do not necessarily pass all the way from their source in the lower lithosphere (or asthenosphere) through to the surface in one rapid step (as implied by Wilson and Head, 2009). Lithospheric barriers caused by rock property changes and/or stress variations do impede or halt kimberlite dyke propagation to form sills. Volcanic models need to account for complex variations in the composition of melt batches, due to contamination and fractionation processes, that rise to surface one after another in relatively short periods of time. Emplacement models must also explain the repeated utilization of the same melt pathways through the crust, allowing magmatic overpressures to build and drive melt beyond the crustal barriers, and eventually form a volcanic pipe at surface.

Acknowledgements

References

Anderson, D.J. and Lindsley, D.H., 1979. The olivine-ilmenite thermometer. Proceedings of the Lunar Science 10th Conference, 493–507.

Andreoli, M., Doucouré, M., Van Bever Donker, J., Brandt, D. and Anderson, N.J.B., 1996. Neotectonics of southern Africa – a review. Africa Geoscience Review, 3 (1), 1–16.

Armstrong, J.P., Wilson, M.R., Barnett, R.L., Nowicki, T. and Kjarsgaard, B.A., 2004. Mineralogy of primary carbonate-bearing hypabyssal kimberlite, Lac de Gras, Slave Province, Northwest Territories, Canada. Lithos, 76, 415–433.

Bailey, D.K., 1984. Kimberlite: "The mantle sample" formed by ultrametasomatism. In: J. Kornprobst, (Editor). Kimberlites I: kimberlites and related rocks. Elsevier. Amsterdam, 323–334.

Bailey, D.K. and Kearns, S., 2002. High-Ti magnetite in some fine-grained carbonatites and the magmatic implications. Mineralogical Magazine, 66, 379–384.

Bailey, D.K. and Woolley, A.R., 1995. Magnetic quiet periods and stable continental magmatism: Can there be a plume dimension? In: Anderson, D.L., Hart, S.R., and Hofmann, A.W (Editors). Plume 2, Terra Nostra, 3, 15–19, Alfred-Wegener-Stiftung, Bonn.

Barnett, W.P., 2006. The Mechanics of Kimberlite Emplacement. Unpublished Doctorate Thesis, University of KwaZulu-Natal, South Africa, 277p.

Beard, A.D., Downes, H., Hegner. E. and Sablukov, S.M., 2000. Geochemistry and mineralogy of kimberlites from the Arkhangelsk region, NW Russia: evidence for transitional kimberlite magma types. Lithos, 51, 47–73.

Becker, M. and Le Roex, A.P., 2006. Geochemistry of South African On- and Off-craton Group I and Group II kimberlites: petrogenesis and source region evolution. Journal of Petrology, 47, 673–703.

Berg, G.W., 1989. The significance of brucite in South African kimberlites. In J. Ross, (Editor). Kimberlite and related rocks, Volume 2: Their mantle/crust setting. Diamonds and diamond Exploration. Geological Society of Australia Special Publication, 14, Blackwell Scientific, Victoria, Australia, 282–296.

Bons, P.D., Arnold, J., Elburg, M.A., Soesoo, A. and van Milligen, B.P., 2004. Melt extraction and accumulation from partially molten rocks. Lithos, 78, 25–42.

Bosch, P.J.A. and Visser, D.J.L., 1993. Geological map of Kimberley, Sheet 2824 (1:250000). Geological Survey of South Africa.

Brett, R.C., Russell, J.K. and Moss, S., 2009. Origin of olivine in kimberlite: Phenocryst or imposter? Lithos, 112S, 201–212.

Clarke, D.B. and Mitchell, R.H., 1975. Mineralogy and petrology of the kimberlite from Somerset island, N.W.T., Canada. Physical Chemistry of the Earth, 9, 123–135.

Clement, C.R., 1975. The emplacement of some diatreme facies. Physical Chemistry of the Earth, 9, 51–59.

Clement, C.R., 1982. A comparative geological study of some major kimberlite pipes in the Northern Cape and Orange Free State. Unpublished Doctorate Thesis, University of Cape Town, South Africa.

Dalton, J.A. and Presnell, D.C., 1998. The continuum of primary carbonatitic-kimberlite melt compositions in equilibrium with lherzolite: data from the system $CaO-MgO-Al_2O_3-SiO_2-CO_2$ at 6 GPa. Journal of Petrology, 39, 1953–1964.

Dasgupta, R. and Hirschmann, M.M., 2006. Melting in the Earth's deep upper mantle caused by carbon dioxide. Nature, 440, 659–662.

Davis, G.L., 1977. Zircons from the mantle. Annual Report of Carnegie Institution, Geophysical Laboratory, Washington, D.C., U.S.A., 896–897.

Dawson, J.B. (1970). The structural setting of African kimberlite magmatism. In: T.N. Clifford and I.G. Gass (Editors). African Magmatism and Tectonics, Oliver and Boyd, Edinburgh, 321–335.

Dawson, J.B., 1994. Quaternary kimberlite volcanism on the Tanzania craton. Contributions to Mineralogy and Petrology, 116, 473–485.

Dawson, J.B. and Hawthorne, J.B., 1973. Magmatic sedimentation and carbonatitic differentiation in kimberlite sills at Benfontein, South Africa. Journal of the Geological Society of London, 129, 61–85.

Delaney, P.T., Pollard, D.D., Ziony, J.I. and McKee, E.H., 1986. Field relations between dikes and joints: Emplacement processes and paleostress analysis. Journal of Geophysical Research, 91, B5, 4920–4938.

De Wit, M., 2007. The Kalahari Epeirogeny and climate change: differentiating cause and effect from core to space. South African Journal of Geology, 110, 367–392.

Donaldson, C.H. and Reid, A.M., 1982. Multiple intrusion of a kimberlite dyke. Transactions of the Geological Society of South Africa, 85, 1–12.

Edgar, A.D. and Chabonneau, H.E., 1993. Melting experiments on a silica-poor, Ca-rich aphanitic kimberlite from 5-10 GPa and their bearing on the sources of kimberlite magmas. American Mineralogist, 87, 1235–1241.

Evans, B.W., 2004. The serpentine multisystem revisited: chrysotile is metastable. International Geology Review, 46, 479–506.

Fedortchouk, Y. and Canil, D., 2004. Intensive variables in kimberlite magmas, Lac de Gras, Canada and implications for diamond survival. Journal of Petrology, 45, 1725–1745.

Field, M. and Scott Smith, B.H., 1999. Contrasting geology and near-surface emplacement of kimberlite pipes in Southern Africa and Canada. Proceedings of the 7th International Kimberlite Conference, Cape Town, 1, 214–216.

Field, M., Stiefenhofer, J., Robey, J.V. and Kurzslaukis, S., 2008. Kimberlite-hosted diamond deposits of southern Africa: A review. Ore Geology Reviews, 34, 33–75.

Gaspar, J.C. and Wyllie, P.J., 1984. The alleged kimberlite-carbonatite relationship: evidence from ilmenite and spinel from Premier and Wesselton Mines and the Benfontein Sill, South Africa. Contributions to Mineralogy and Petrology, 85, 133–140.

Greeff, G.J., 1968. Fracture systems and the kimberlite intrusions of Griqualand West. Unpublished M.Sc. thesis, University of Stellenbosch, 126pp.

Gudfinnsson, G.H. and Presnall, D.C., 2005. Continuous gradations among primary carbonatitic, kimberlitic, melilitic, basaltic, picritic, and komatiitic melts in equilibrium with garnet lherzolite at 3-8 GPa. Journal of Petrology, 46, 1645–1659.

Hanson, E.K., Moore, J.M., Bordy, E.M., Marsh, J.S. and Howarth, G., 2009. Cretaceous erosion in central South Arica: Evidence from upper-crustal xenoliths in kimberlite diatremes. South African Journal of Geology; 112 (2), 125–140.

Harris, M., Le Roex, A. and Class, C. 2004. Geochemistry of the Uintjiesberg kimberlite, South Africa: petrogenesis of an off-craton, Group I, kimberlite. Lithos, 74, 149–165.

Hawthorne, J.B., 1968. Kimberlite sills. Transactions of the Geological Society of South Africa, 71, 291–311.

Hawthorne, J.B., 1975. A model of a kimberlite pipe. Physics and Chemistry of the Earth, 9, 1–15.

Henderson, P., 1970. The significance of the mesostasis of basic layered igneous rocks. Journal of Petrology, 11, 243–473.

Hill, D.R.H., 1977. Field relationships and petrography of the kimberlite sill complex at the 40 metre level of Wesselton mine, Kimberley, South Africa. Unpublished B.Sc Honours project, University of Cape Town, South Africa.

Jelsma, H.A., De Wit, M.J., Thiart, C., Dirks, P.H.G.M., Viola, G., Basson, I.J. and Anckar, E., 2004. Preferential distribution along transcontinental corridors of kimberlites and related rocks of Southern Africa. South African Journal of Geology, 107, 1, 301–324.

Jelsma, H., Barnett, W.P., Richards, S. and Lister, G. (2009). Tectonic setting of kimberlites. doi:10.1016/j.lithos.2009.06.030

Jerram, D.A., Cheadle, M.J. and Philpotts, A.R., 2003. Quantifying the building blocks of igneous rocks: are clustered crystal frameworks the foundation? Journal of Petrology, 44, 2033–2051.

Kavanagh, J. and Sparks, R.S.J., 2009. Temperature changes in ascending kimberlite magmas. Earth and Planetary Science Letters, 286, 404–413.

Kavanagh, J.L., Menand, T. and Sparks R.S.J., 2006. An experimental investigation of sill formation and propagation in layered elastic media. Earth and Planetary Science Letters 245, 799–813.

Kelly, D.S., Karson, J.A., Fruh-Green, G.L., Yoerger, D.R., Shank, T.M., Olson, E.J., Proskurowski, G., Jakuba, M., Bradley, A., Larson, B., Ludwig, K., Glickson, D., Buckman, K., Bradley, A.S., Brazelton, W.J., Roe, K., Elend, M.J., Delacour, A., Bernasconi, S.M., Lilley, M.D., Baross, J.A., Summons, R.E. and Sylva, S.P., 2005. A serpentine-hosted ecosystem: the Lost City Hydrothermal Field. Science, 307, 1428–1434.

Komar, P.D., 1972. Flow differentiation in igneous dikes and sills: profiles of velocity and phenocrysts concentration. Bulletin of the Geological Society of America, 83, 3443–3448.

Le Maitre, R.W., 2002. Igneous Rocks: a Classification and Glossary of Terms. Cambridge University Press, Cambridge, United Kingdom, 236pp.

Le Roex, A.P., Bell, D.R. and Davis, P., 2003. Petrogenesis of group I kimberlites from Kimberley, South Africa: evidence from bulk-rock geochemistry. Journal of Petrology, 44, 2261–2286.

Lister, J.R. and Kerr, R.C., 1991. Fluid-mechanical models of crack propagation and their application to magma transport in dykes. Journal of Geophysical Research, 96, 10049–10077.

McMahon, B. and Haggerty, S., 1984. The Benfontein kimberlite sills: magmatic reactions and high intrusion temperatures. American Journal of Science, 284, 893–941.

Menand, T., 2008. The mechanics and dynamics of sills in layered elastic rocks and their implications for the growth of laccoliths and other igneous complexes. Earth and Planetary Science Letters, 267, 93–99.

Mitchell, R.H., 1984. Mineralogy and origins of carbonate-rich segregations in a composite kimberlite sill. Neues Jahrbuch Miner.abh., 150, 185–197.

Mitchell, R.H., 1986. Kimberlites: mineralogy, geochemistry, and petrology. Plenum Press, New York, N.Y. U.S.A., 442pp.

Mitchell, R.H., 1991. Accessory Rare Earth, Strontium, Barium, and Zirconium minerals in the Benfontein and Wesselton Calcite Kimberlites, South Africa. In: H.O.A. Meyer and O.H. Leonardos (Editors). Proceedings of the 5th International Kimberlite Conference, Volume 1: Kimberlites, related rocks and mantle xenoliths, Companhia de Pesquisa de Recursos Minerais, Brasilia, Special Publication 1A, 115–128.

Mitchell, R.H., 1995. Kimberlite, orangeites, and Related Rocks. Plenum Press, New York, N.Y., 410pp.

Mitchell, R.H., 2005. Carbonatites and carbonatites and carbonatites. Canadian Mineralogist 43, 2049–2068.

Mitchell, R.H., 2008. Petrology of hypabyssal kimberlites: relevance to primary compositions. Journal of Volcanology and Geothermal Research, 174, 1–8.

Mitchell, R.H., Skinner, E.M.W. and Scott Smith, B.H., 2009. Tuffisitic kimberlites from the Wesselton Mine, South Africa: Mineralogical characteristics relevant to their formation. Lithos, 112, 452–464.

Moore, A., Blenkinsop, T. and Cotterill, F. (2008). Controls on post-Gondwana alkaline volcanism in Southern Africa. Earth and Planetary Science Letters, 268, 151–164.

Nixon, P.H. and Kresten, P., 1973. Butha-Buthe dyke swarm and associated kimberlite blows. In: P.H. Nixon (Editor). Lesotho Kimberlites. Lesotho National Development Corp., 197–206.

Otto, J.W. and Wyllie, P.J., 1993. Relationships between silicate melts and carbonate-precipitating melts in $CaO-MgO-SiO_2-CO_2-H_2O$ at 2 kbar. Mineralalogy and Petrology, 48, 343–365.

Pollard, D.D., 1973. Derivation and evaluation of a mechanical model for sheet intrusions. Tectonophysics, 19, 233–269.

Price, S.E., Russell, J.K. and Koplova, M.G., 2000. Primitive magma from the Jericho Pipe, NWT, Canada: constraints on primary kimberlite melt chemistry. Journal of Petrology, 41, 789–808.

Priestley, K., McKenzie, D. and Debayle, E., 2006. The state of the upper mantle beneath southern Africa. Tectonophysics, 416, 101–112.

Rubin, A.M., 1995. Propagation of magma-filled cracks. Annual Reviews of Earth and Planetary Sciences, 23, 287–336.

Schwindinger, K.R., 1999. Particle dynamics and aggregation of crystals in a magma chamber with application to Kilaueo Iki olivines. Journal of Volcanology and Geothermal Research, 88, 209–238.

Shee, S.R., 1984. The oxide minerals of the Wesselton mine kimberlite, Kimberley, South Africa. In: J. Kornprobst (Editor). Kimberlites I: kimberlites and related rocks. Elsevier. Amsterdam, the Netherlands, 59–73.

Shee, S.R., 1985. The petrogenesis of the Wesselton mine kimberlite, Kimberley, Cape Province, Republic of South Africa. Unpublished PhD thesis, University of Cape Town, South Africa, 220pp + appendices.

Shee, S.R., Clement, C.R. and Skinner, E.M.W., 1991. The petrology of the Wesselton kimberlite sills, Kimberley, Cape Province, South Africa. Proceedings of the 5th International Kimberlite Conference, Volume 1: Kimberlites, related rocks and mantle xenoliths, Companhia de Pesquisa de Recursos Minerais, Brasilia, Special Publication 1A, 98–114.

Smith, C.B., 1983. Rubidium-strontium, uranium-lead, samarium-neodymium isotopic studies of kimberlite and selected mantle-derived xenoliths. Unpublished PhD thesis. University of Witwatersrand, Johannesburg South Africa.

Sparks, R.S.J., Baker, L., Brown, R., Field, M., Schumacher, J., Stripp, G. and Walters, A., 2006. Dynamical constraints on kimberlite volcanism. Journal of Volcanology and Geothermal Research 155, 18–48.

Sparks, R.S.J., Brooker, R.A., M. Field, M. Kavanagh, J. Schumacher, J.C., Walter, M.J. and White, J., 2009. The nature of erupting kimberlite melts. Lithos, 112S, 429–438.

Stripp, G.R., Field, M., Schumacher, J.C. and Sparks, R.S.J., 2006. Post Emplacement Serpentinization and related Hydrothermal Metamorphism in a Kimberlite from Venetia, South Africa. Journal of Metamorphic Geology 24, 515–534.

Tankard, A.J., Jackson, M.P., Eriksson, K.A., Hobday, D.K., Hunter, D.R. and Minter, W.E.L., 1982. Crustal Evolution of Southern Africa: 3.8 Billion Years of Earth History. Springer-Verlag, New York, United States of America, 523pp.

Vearncombe, S. and Vearncombe, J.R., 2002. Tectonic controls on kimberlite location, southern Africa. Journal of Structural Geology, 24, 1619–1625.

Visser, D.J.L., 1984. Geological map of the Republics of South Africa, Transkei, Bophuthatswana, Venda and Ciskei and the Kingdoms of Lesotho and Swaziland (1: 000 000), gravity edition. Geological Survey of South Africa.

Wagner, P.A., 1914. The diamond field of Southern Africa. Transvaal Leader, 347pp.

Wilson L. and Head III, J.W., 2007. An integrated model of kimberlite ascent and eruption. 447, 53–57.

Editorial handling: J.M. Barton Jr.